Journal of Medicinal Chemistry

pubs.acs.org/jmc Article

Diflunisal Derivatives as Modulators of ACMS Decarboxylase Targeting the Tryptophan−Kynurenine Pathway

Yu Yang, Timothy Borel,[▽] Francisco de Azambuja,[▽] David Johnson, Jacob P. Sorrentino, Chinedum Udokwu, Ian Davis, Aimin Liu,* and Ryan A. Altman*

Cite This: *J. Med. Chem.* 2021, 64, 797−811 Read Online

ACCESS | Metrics & More | Article Recommendations | Supporting Information

ABSTRACT: In the kynurenine pathway for tryptophan degradation, an unstable metabolic intermediate, α-amino-β-carboxymuconate-ε-semialdehyde (ACMS), can nonenzymatically cyclize to form quinolinic acid, the precursor for de novo biosynthesis of nicotinamide adenine dinucleotide (NAD^+). In a competing reaction, ACMS is decarboxylated by ACMS decarboxylase (ACMSD) for further metabolism and energy production. Therefore, the inhibition of ACMSD increases NAD^+ levels. In this study, an Food and Drug Administration (FDA)-approved drug, diflunisal, was found to competitively inhibit ACMSD. The complex structure of ACMSD with diflunisal revealed a previously unknown ligand-binding mode and was consistent with the results of inhibition assays, as well as a structure−activity relationship (SAR) study. Moreover, two synthesized diflunisal derivatives showed half-maximal inhibitory concentration (IC_{50}) values 1 order of magnitude better than diflunisal at 1.32 ± 0.07 μM (**22**) and 3.10 ± 0.11 μM (**20**), respectively. The results suggest that diflunisal derivatives have the potential to modulate NAD^+ levels. The ligand-binding mode revealed here provides a new direction for developing inhibitors of ACMSD.

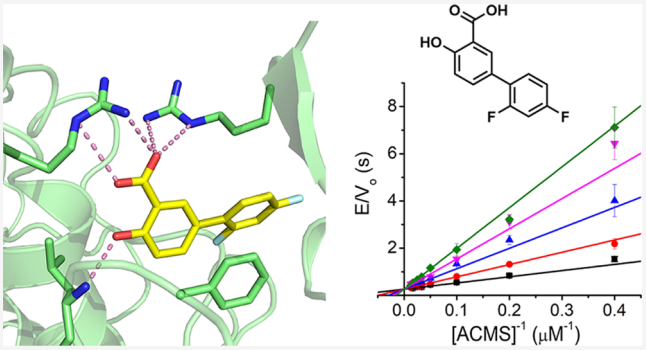

INTRODUCTION

Nicotinamide adenine dinucleotide, $NAD(P)^+$, is an essential redox cofactor across all kingdoms of life. The de novo synthesis of NAD^+ in mammals and some bacteria starts from the tryptophan−kynurenine degrading pathway (Figure 1). A transient metabolite of the pathway, α-amino-β-carboxymuconate-ε-semialdehyde (ACMS), in its enol tautomer form, is a metabolic intermediate at the crossroad between NAD^+ biosynthesis and energy production.[1] ACMS is unstable and can nonenzymatically cyclize to form quinolinic acid (QUIN), a precursor for NAD^+ synthesis. In a competing pathway, the β-carboxylic group of ACMS can be enzymatically removed by a Zn-dependent decarboxylase (ACMSD) to form α-amino-muconate semialdehyde (2-AMS) for further enzyme-mediated catabolism. Therefore, the QUIN levels are directly regulated by ACMSD and could become elevated by inhibiting ACMSD. The regulation of NAD^+ levels through modulating ACMSD activity has been experimentally demonstrated in mice, as high expression of ACMSD led to a niacin-dependent phenotype.[2,3] QUIN is also an endogenous agonist of NMDA receptors.[4] Misregulated QUIN production is linked to a wide range of neuropsychiatric disorders.[5−8] In bacteria, such as *Pseudomonas fluorescens*, biodegradation of 2-nitrobenzoic acid can enter the kynurenine pathway, though this substrate avoids the first two steps.[9]

ACMSD occupies a central position in both metabolic pathways. The discovery of the bacterial protein has facilitated biochemical and structural studies. ACMSD belongs to the amidohydrolase superfamily,[10] and it is a prototypic member for a large subgroup of decarboxylases and hydratases.[10,11] This enzyme performs a metal-mediated, O_2-independent, non-oxidative decarboxylation reaction,[12] which proceeds through a metal-bound hydroxide.[13] The crystal structures of ACMSD from both human and *P. fluorescens* have been previously determined.[11,14] ACMSD is catalytically inactive in the monomer form and active in the homodimer form because the neighboring subunit contributes one of the two substrate-binding arginine residues.[15] The enzyme shows a protein concentration-dependent activity, as its quaternary structure is in a dynamic equilibrium among the monomer, dimer, and higher-order oligomeric states.[16] Pyridine-2,6-dicarboxylic (PDC) acid is a biochemically established inhibitor (Scheme 1A).[14] In the crystal structure of human ACMSD (hACMSD)

Received: October 7, 2020
Published: December 28, 2020

https://dx.doi.org/10.1021/acs.jmedchem.0c01762
J. Med. Chem. 2021, 64, 797−811

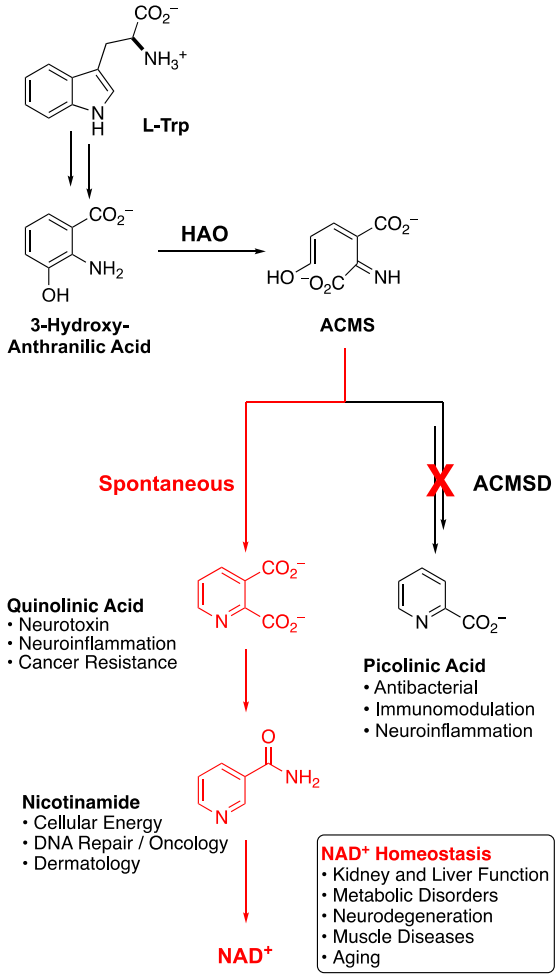

Figure 1. Inhibition of ACMSD increases NAD^+ biosynthesis.

in complex with PDC,[14] or another inhibitor 1,3-dihydroxyacetone phosphate (DHAP),[17] the inhibitors are located near the zinc center and are recognized by a substrate-binding residue, Arg47. A phthalate ester, mono(2-ethylhexyl)phthalate, also reportedly reversibly inhibited ACMSD activity and increased QUIN levels as detected in the urinary excretion of rats.[18]

In 2018, an effective, nanomolar inhibitor of ACMSD, TES-1025, was developed based on the published structural information in complex with PDC and DHAP.[17,19] In cellular systems, inhibiting ACMSD activity increased the NAD^+ concentration and enhanced QUIN formation. Using in vivo knockout systems and pharmacological intervention with TES-1025, further comprehensive investigations demonstrated that the inhibition of ACMSD activity similarly increased the NAD^+ concentration and sirtuin activity and improved the mitochondrial function in *Caenorhabditis elegans*, mouse, and human tissues, such as liver and kidney, in which ACMSD is highly expressed.[3] How TES-1025 binds ACMSD and its mechanism of inhibition have not been determined.

Compared with developing an entirely new drug, expanding new uses of Food and Drug Administration (FDA)-approved drugs can be much less costly and can deepen the understanding of the drugs in the human body. Here, we screened FDA-approved drugs to develop inhibitors of ACMSD. Diflunisal was identified to inhibit ACMSD, and the mechanism of inhibition was characterized. Diflunisal

Scheme 1. (A) Chemical Structures of Reported Inhibitors of ACMSD; (B) Virtual Screening Delivered Computational Hits That Bound the Catalytically Active Zn Center Using a Carboxylate Group (Protein Data Bank (PDB) Entry: 4IH3); (C) Computationally Predicted Docking Pose for Diflunisal Predicts That the Salicylate Head Interacts near Catalytically Active Zn^{2+}, While the Difluorinated Aryl Ring Projects through a Hydrophobic Tunnel

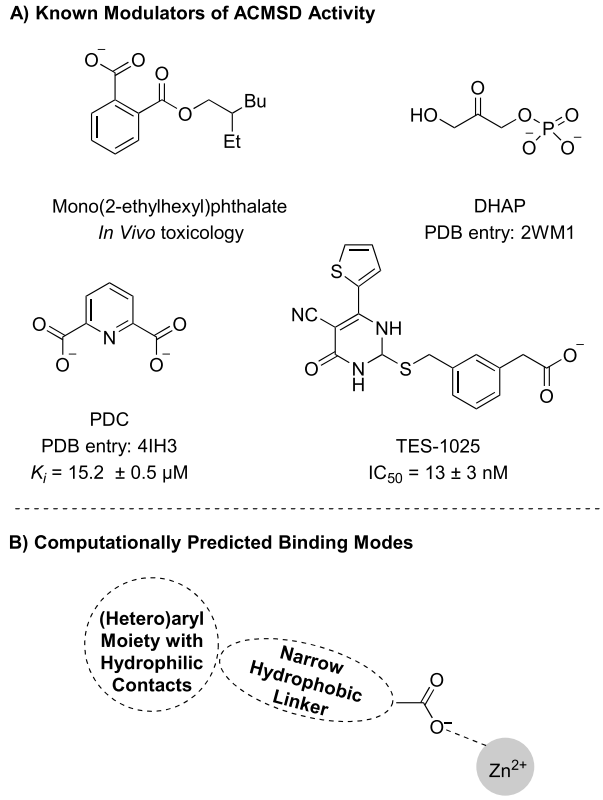

derivatives were synthesized to elucidate the functional groups and improve overall inhibition. Cocrystal structures of ACMSD with the new inhibitors revealed a previously

https://dx.doi.org/10.1021/acs.jmedchem.0c01762
J. Med. Chem. 2021, 64, 797−811

unknown inhibitor-binding mode in the active site of ACMSD, which involved residues distant from the zinc center. These findings provide a new direction for developing ACMSD inhibitors.

RESULTS

Molecular Modeling of FDA-Approved Drugs in the Active Site of ACMSD. A library of roughly 5000 FDA-approved drugs was screened for binding at the active site of human ACMSD[14] by rigid-receptor docking using Glide[20−23] at successively increasing precision levels. The highest scoring 62 unique compounds were chosen for refinement using Prime molecular mechanics-generalized Born surface area (MM-GBSA),[23−25] and the refined ligand-bound structures, along with the chemical structures, fell into several clusters of compounds that potentially bind human ACMSD: bisphosphonates, citrates, ibuprofen-derived nonsteroidal anti-inflammatory drugs (NSAIDs, cyclooxygenase inhibitors),[26,27] salicylate-derived NSAIDs, and other miscellaneous compounds (Table S1). The docking models suggested that most of these compounds might bind ACMSD in the active site through a carboxylate that interacts with the zinc ion (Scheme 1B). A linear lipophilic stem that sticks through the active pocket might also help engage the enzyme. From each cluster, structurally diverse compounds were acquired. Depending on the group, 1−6 compounds were selected as representative of possible structural diversity, and a total of 14 representative compounds was chosen from each cluster to test the inhibition of ACMSD activity (Scheme S1 and Table 1).

Table 1. Initial Assessment of FDA-Approved Drugs Recommended by the Computational Docking Study

compounds (1 mM)	PA (%)	QUIN (%)
control (ACMSD)	83.6 ± 3.1	16.4 ± 2.9
risedronate	82.7 ± 7.1	17.4 ± 5.2
alendronic acid	99.6 ± 1.9	0.43 ± 0.24
ibandronate	98.7 ± 2.2	1.29 ± 0.18
citric acid	78.6 ± 7.8	21.4 ± 2.9
ibuprofen	75.4 ± 1.4	24.6 ± 1.7
fenoprofen	75.9 ± 3.0	24.1 ± 4.5
ketoprofen	76.0 ± 1.2	24.0 ± 1.7
fenbufen	78.2 ± 2.4	21.8 ± 1.3
mitiglinide	98.7 ± 6.4	1.26 ± 0.55
naproxen	88.9 ± 3.3	11.1 ± 1.7
tolmetin	85.1 ± 2.9	14.9 ± 1.5
aminohippuric acid	95.0 ± 3.4	5.03 ± 0.77
pregabalin	97.0 ± 3.5	2.98 ± 0.69
diflunisal (**1**)	6.9 ± 0.3	93.1 ± 3.2

Discovery of Diflunisal as an Inhibitor of Human ACMSD. To rapidly screen compounds prior to conducting more comprehensive inhibition studies, we developed an enzymatic method to assess the inhibition of human ACMSD by quantitation of the relevant kynurenine products by high-performance liquid chromatography (HPLC). Both the substrate (ACMS, $t_{1/2}$ = 46 min at pH 7.0 and 20 °C) and the immediate product (2-AMS, $t_{1/2}$ = 35 s at pH 7.0 and 20 °C) of the ACMSD reaction are unstable,[28] and spontaneously decay to QUIN and picolinic acid (PA), respectively. Thus, in this enzymatic assay, the production of PA serves as a direct reporter of ACMSD activity, as the decarboxylation product 2-AMS undergoes cyclization to form PA (Table 1). Alternatively, the inhibition of ACMSD would facilitate the formation of QUIN. In practice, the reaction mixtures contained 1 mM of test compounds and were run overnight to ensure complete formation of the decay products. Then, QUIN and PA were separated and quantitated from the reaction mixtures by HPLC.

As shown in Table 1, compared with the control sample (no inhibitor), 13 of the 14 candidates showed no significant differences in the distribution of PA vs QUIN, indicating that they had no apparent inhibition of ACMSD activity, and thus, these computational hits were not pursued further. The presence of the pain reliever, diflunisal (**1**), however, generated significant quantities of ACMS-derived QUIN (93%), and only a small amount of the decarboxylation product-derived PA (7%), indicating that ACMSD was nearly completely inhibited by diflunisal under the assay conditions. At this point, reinspection of the docked pose predicted that the phenol presented toward the catalytic Zn^{2+}, while the carboxylate engaged the N−H of Trp191. Furthermore, the difluorinated ring was predicted to protrude through a narrow hydrophobic tunnel composed of Phe46, Val78, Met178, Met180, and Trp191 (Scheme 1C).

Determination of Structure−Activity Relationship (SAR) for the Inhibition of ACMSD by Diflunisal Derivatives. To further probe the structural determinants required for the inhibition of ACMSD, a structure−activity relationship (SAR) study was pursued using a molecular simplification approach. Diflunisal contains two phenyl rings in which one ring (A) has a hydroxyl group and a carboxylate substituent, and the other ring (B) has two fluoro substituents (Table 2). Like the previously reported inhibitors,[14,15,17,19] diflunisal shares the common feature of a carboxylate group. The SAR assay for diflunisal inhibiting ACMSD activity was performed by systematically altering each of the substituents of diflunisal and measuring the inhibition of each derivative (Table 2). For ring A, the carboxylate and hydroxyl groups were either removed separately (**2** and **3**) or substituted with CH_2OH (**4**), $COOCH_3$ (**5**), and $CONH_2$ (**6**). For ring B, the fluorine atoms were substituted with hydrogen (**7**, **8**, **10**) or shifted to the meta position (**9**). Additionally, analogues **11**−**13** explored the significance of the B ring.

The preparation of compounds **4**−**6**, bearing distinct functional groups on the A ring, was accessed from diflunisal, itself, via reduction, esterification, and amidation reactions (Scheme 2A). The synthetic route for accessing diflunisal derivatives (**7**−**11**) generally involved Suzuki coupling of 5-bromosalicylic acid (**14**) or the corresponding ester (**15**) with properly substituted arylboronic acids under aqueous (aq) conditions (Scheme 2B).[29]

As shown in Table 2, the reaction mixtures containing **2**−**6** produced similar amounts of PA compared with the control, suggesting no inhibition of ACMSD activity. As such, both the carboxylate and hydroxyl groups are essential for inhibiting ACMSD. Diflunisal derivatives with a modified B ring (**7**−**11**) inhibited ACMSD similarly as diflunisal. Therefore, the positioning of the fluoro groups on the B ring did not significantly contribute to the inhibition of ACMSD. Because the A ring of diflunisal bears the salicylic acid (2-hydroxybenzoic acid) moiety, the active component of aspirin, salicylic acid (**12**) itself was included in this set of experiments as a simplified analogue. Interestingly, even with both the carboxylate and hydroxyl groups of the A ring, no inhibition was observed (Table 2), though a more sensitive assay did

https://dx.doi.org/10.1021/acs.jmedchem.0c01762
J. Med. Chem. 2021, 64, 797−811

Table 2. Metabolic Flux Ratio of PA and QUIN

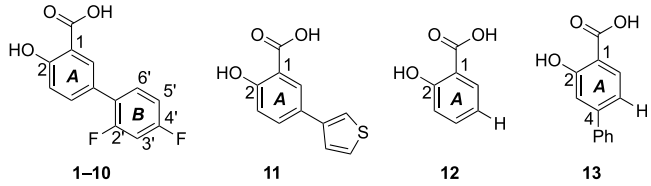

#	ring A	ring B	PA (%)	QUIN (%)
control (no inhibitor)			83.6 ± 3.1	16.4 ± 2.9
diflunisal (**1**)	1 = COOH; 2 = OH	2′ = F; 4′ = F	6.9 ± 0.3	93.1 ± 3.2
2	1 = COOH; 2 = H	2′ = F; 4′ = F	77.0 ± 1.3	23.0 ± 0.1
3	1 = H; 2 = OH	2′ = F; 4′ = F	73.3 ± 0.6	26.7 ± 2.0
4	1 = CH_2OH; 2 = OH	2′ = F; 4′ = F	82.3 ± 0.2	17.7 ± 0.3
5	1 = $COOCH_3$; 2 = OH	2′ = F; 4′ = F	83.4 ± 0.2	16.6 ± 0.2
6	1 = $CONH_2$; 2 = OH	2′ = F; 4′ = F	82.1 ± 0.6	17.9 ± 0.6
7	1 = COOH; 2 = OH	2′ = H; 4′ = F	6.0 ± 0.4	94.0 ± 5.5
8	1 = COOH; 2 = OH	2′ = F; 4′ = H	5.3 ± 0.1	94.7 ± 0.6
9	1 = COOH; 2 = OH	2′ = H; 3′ = F; 4′ = H	2.9 ± 0.3	97.1 ± 3.1
10	1 = COOH; 2 = OH	2′ = H; 4′ = H	5.1 ± 0.1	94.9 ± 0.4
11	1 = COOH; 2 = OH	3-thiophene	0.82 ± 0.38	99.2 ± 3.1
12	1 = COOH; 2 = OH	none	100 ± 2.1	ND
13	1 = COOH; 2 = OH	4 = Ph	27.2 ± 2.3	73 ± 11

Scheme 2. Preparation of Compounds 4–11

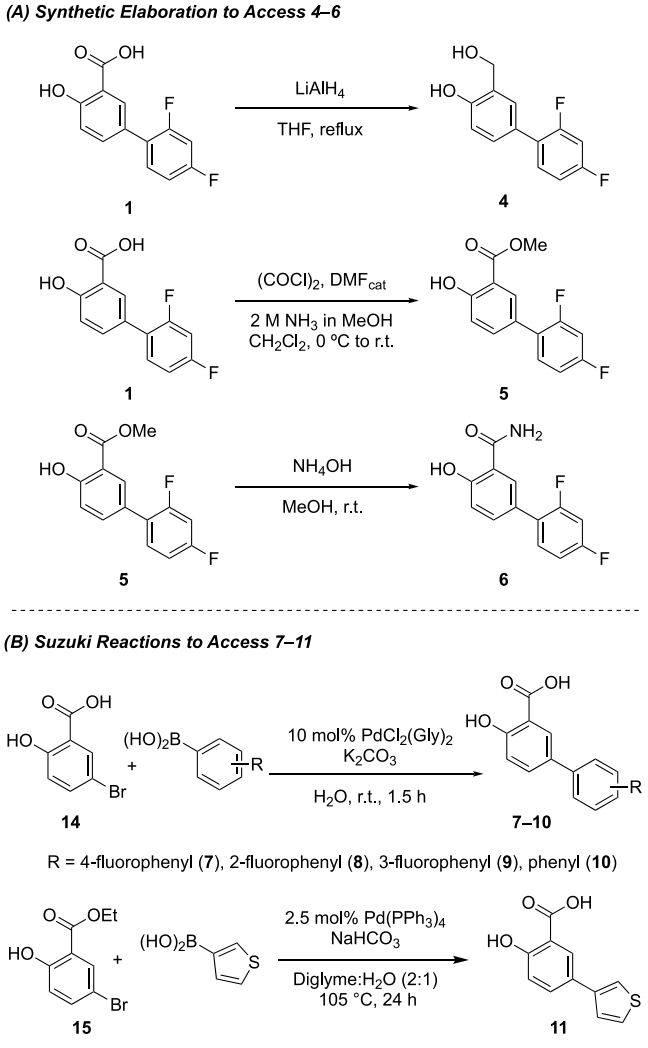

detect weak inhibition with an half-maximal inhibitory concentration (IC_{50}) value above 500 μM (data not shown). These findings suggest that the B ring moiety was also essential for effectively inhibiting ACMSD activity. Derivative **13**, in which the B ring was switched from the meta- to para-position, demonstrated poor inhibition, with less than one-third of PA in the mixture relative to diflunisal.

It has been previously shown that the active-site structures of human ACMSD and *P. fluorescens* ACMSD (*pf*ACMSD) are superimposable and nearly indistinguishable.[14] The two proteins also share 56% sequence identity. However, the bacterial enzyme is more robust and produces better quality crystals. Thus, *pf*ACMSD was used to pursue inhibitor-bound complex structures that would facilitate studying the inhibitory mechanism. The crystals of ACMSD were soaked with the mother liquor containing diflunisal to obtain an inhibitor-bound complex structure. The ACMSD–diflunisal complex structure (Figure 2A) was obtained and refined to a resolution of 2.17 Å (Table 3). The overall structure of the ACMSD–diflunisal complex was similar to the ligand-free ACMSD structure,[10] as indicated by a root-mean-square deviation (RMSD) value of 0.272 Å for all Cα carbons.

The essential residues involved in the ACMSD-catalyzed reaction are Arg51 and Arg239* (* denotes a residue from a neighboring subunit), with each Arg binding a carboxylic group of the substrate[15] and His228, which functions as an active-site acid/base catalyst.[13] Comparing the ligand-free and ligand-bound structures, the three Zn-binding histidine residues, as well as His228 and Arg239* in the diflunisal-bound structure, show no conformational change. Thus, the inhibitory mechanism may involve the competitive binding of diflunisal to the substrate (ACMS) binding site. However, the diflunisal-bound structure reveals significantly distinct protein–ligand interactions compared to the previously observed ligand-bound structures[14,17] or those predicted in our virtual screen (Scheme 1C and Figure S2). As shown in Figure 2B, Arg51 and Arg247* rotate from the active-site pocket toward the outside and form salt bridges with the carboxylate group of diflunisal. Moreover, upon diflunisal binding, the side- chain of

https://dx.doi.org/10.1021/acs.jmedchem.0c01762
J. Med. Chem. 2021, 64, 797–811

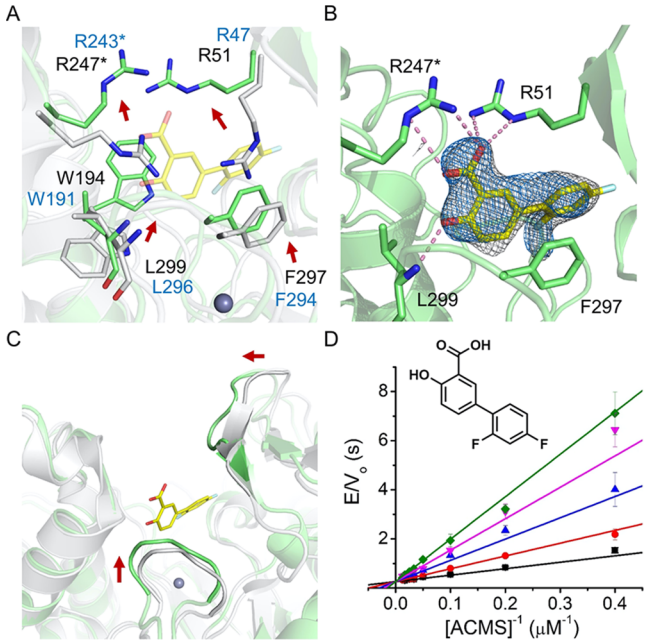

Figure 2. Crystal structure of *pf*ACMSD in complex with diflunisal (PDB entry: 7K12). (A) Enlarged figure shows the residues (green sticks) that interact with diflunisal (yellow sticks). The $2F_o - F_c$ (gray) and omit $F_o - F_c$ (marine) maps for diflunisal (**1**) are contoured at 1 σ and 2.5 σ, respectively. The aligned residues from hACMSD are labeled in blue for comparison. (B) Superimposed ACMSD−diflunisal complex structure (green) with the ligand-free ACMSD structure (gray, PDB entry: 2HBV). The substrate is set with 50% transparency for better presentation. (C) Two loop regions move toward diflunisal (**1**). (D) Competitive inhibition of human ACMSD measured at 1.3, 5, 10, 16, and 22.5 μM of diflunisal (**1**) (black, red, blue, pink, and green traces, respectively).

Trp194 flips over, while Phe297 and Leu299 also move closer to the ligand, indicating a dynamic nature of these residues upon the ligand binding. The backbone of Leu299 forms a H-bond with the hydroxyl group of diflunisal at 3.2 Å, and Phe297 engages in a $\pi-\pi$ stacking interaction with the fluorinated phenyl (B) ring of diflunisal (Figure 2A). These experimentally determined protein−ligand interactions rationalize why changing the orientation of the B ring (**13**) weakened the inhibitory activity. Specifically, binding of diflunisal induced two loop regions consisting of residues of 47−53 (loop β3*)[11] and 295−300 to move toward the active site (Figure 2C). The salt bridge formed between the carboxylate group with Arg51 and Arg247*, as well as the H-bond between the hydroxyl group of the A ring and the backbone of Leu299, agree well with the SAR data, which found that both groups are essential for inhibiting hACMSD (Table 2). Moreover, our kinetic analysis indicated that diflunisal is a competitive inhibitor of hACMSD, with a K_i value of 2.56 ± 0.56 μM (Figure 2D). The competitive inhibition mode is consistent with the structural findings.

The diflunisal-bound ACMSD structure represents a new inhibitor-binding mode for ACMSD but aligns well with our predicted substrate-binding mode described in previous studies (Scheme 3).[15] Specifically, the ligand does not engage the active-site zinc center. This mode is characterized by two active-site arginines interacting with the carboxylate groups of the ligand, preventing it from directly ligating the zinc ion, and by doing so, retaining the zinc-bound hydroxide to activate the substrate. As described above, the ligand-binding process also invokes loop movement in the active site. The ligand-

Table 3. X-ray Diffraction Data Collection and Refinement Statistics

	ACMSD in complex with diflunisal	ACMSD in complex with **11**
PDB code	7K12	7K13
data collection		
space group	$P6_122$	$C222_1$
cell dimensions *a*, *b*, *c* (Å)	93.6, 93.6, 445.7	105.0, 150.6, 153.7
σ, β, γ (deg)	90, 90, 120	90, 90, 90
resolution	50−2.17 (2.21−2.17)[a]	50−1.83 (1.86−1.83)
no. of observed reflections	532 757 (62 641)	521 742 (106 608)
redundancy	8.5 (8.4)	4.9 (4.8)
completeness (%)	100.0 (99.7)	99.7 (98.8)
$I/\sigma(I)$	15.3 (1.3)	16.9 (1.2)
R_{merge} (%)[b]	13.2 (95.7)	11.2 (93.1)
$CC_{1/2}$[c]	0.99 (0.82)	0.99 (0.74)
refinement[d]		
R_{work} (%)	20.1	19.1
R_{free} (%)	23.1	21.9
RMSD bond length (Å)[e]	0.007	0.007
RMSD bond angles (deg)	0.938	0.829
Ramachandran statistics[f]		
preferred (%)	96.4	98.2
allowed (%)	3.0	1.7
outliers (%)	0.6	0.1
average *B*-factor (Å^2)		
protein/atoms	46.8/5191	33.0/7796
Zn/atoms	68.6/1	28.3/3
ligands/atoms	57.59/44	46.5/15
solvent/atoms	49.5/422	38.0/812

[a]Values in parentheses are for the highest resolution shell. [b]$R_{merge} = \sum_{hkl}\sum_i|I_i(hkl) - \langle I(hkl)\rangle|/\sum_{hkl}\sum_i I_i(hkl)$, in which the sum is over all of the *i* measured reflections with equivalent miller indices *hkl*; $\langle I(hkl)\rangle$ is the averaged intensity of these *i* reflections, and the grand sum is over all measured reflections in the data set. [c]According to Karplus and Diederichs.[30] [d]All positive reflections were used in the refinement. [e]According to Engh and Huber.[31] [f]Calculated using MolProbity.[32]

Scheme 3. Proposed Binding Mode of ACMS in the Active Site of ACMSD (PDB Entry: 4IH3)

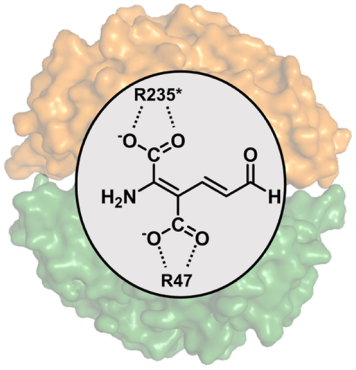

https://dx.doi.org/10.1021/acs.jmedchem.0c01762
J. Med. Chem. 2021, 64, 797−811

interacting residues, Arg47, Arg243*, Phe294, and Leu296, are conserved in human ACMSD (Figure S1).

Moreover, the structure of ACMSD in complex with isosteric analogue **11** was obtained by soaking the inhibitor into the protein crystals. The structure was refined to a 1.83 Å resolution. In principle, compound **11** and diflunisal bind to ACMSD similarly, though some noticeable differences were observed. The density map in Figure 3A shows how **11** binds

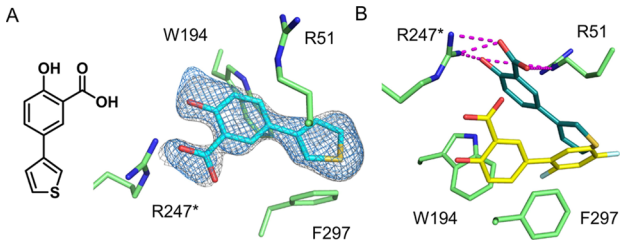

Figure 3. Crystal structure of ACMSD in complex with synthetic compound **11** (PDB entry: 7K13). (A) Electron density maps of $2F_o - F_c$ (gray) and omit $F_o - F_c$ (marine) of **11** are contoured at 1.0 σ and 2.5 σ, respectively. (B) Superimposed structural illustration showing the binding modes of diflunisal (yellow sticks) and **14** (cyan sticks).

to ACMSD in the active site. Upon binding of **11**, the conformations of Arg51, Arg247*, and Trp194 adopt orientations similar to those that were observed in the diflunisal-bound ACMSD structure. However, the orientation of A ring was rotated approximately 45° and was further away from the active-site pocket compared to the diflunisal-bound ACMSD complex (Figure 3B). Although Arg247* engaged **11** at 3.0 Å, the distance of Arg51 to **11** was ca. 5 Å, indicating a weaker interaction with this residue.

Improvement of the Inhibition of Diflunisal Derivatives. Based on the initial round of the SAR data, inhibitory assays, and structural information, a second generation of inhibitors was designed with a conserved salicylate A ring, but with further modifications of the B ring to improve the inhibitory effect (Table 4, compounds **16**–**23**, **26**, **27**). These diflunisal derivatives were generally designed to probe nearby hydrophobic contacts and H-bond network in the ligand-binding pocket to engage the side-chain amide interactions. We synthesized **16** and **17** via Suzuki cross-coupling reactions of salicylate **14** with cycloalkenyl boronic acids (Scheme 4A), and reduction of the cycloalkenes using $Pd/C/H_2$ afforded the corresponding cycloalkanes (**18**, **19**). Tricyclic compounds **20**–**23** and intermediates **24** and **25** were also generated from Suzuki cross-coupling reactions (Scheme 4B,C). From intermediates **24** and **25**, reductive cleavage of the benzyl ether and reduction of the aldehyde afforded alcohol-containing derivatives **26** and **27**, respectively.

As described earlier, an HPLC-based assay was devised to quickly determine whether the new diflunisal derivatives would inhibit ACMSD activity (Table S2). Among **16**–**27**, all of these synthetic diflunisal derivatives showed significant inhibition with the exception of **26** showing a modest inhibition. We then measured the IC_{50} values of these compounds and summarized in Table 4. The results show several trends. Compared to diflunisal (**1**), derivatives **7** and **8** that lacked the para- or ortho-fluorine atoms displayed ~3-fold lower IC_{50} values, indicating that the para-fluorine atom disfavors inhibition and the ortho-fluorine atom minimally influences inhibition. Bicyclic derivatives **16**–**19** showed comparable or higher IC_{50} values than diflunisal, resulting from a similar binding mode of **11** and diflunisal (**1**) in ACMSD (Figures 2 and 3). Taking **10**, **17**, and **19** together, the IC_{50} values increase with the degree of saturation of the B ring. This observation indicates that the aromaticity and planarity of the B ring are beneficial for the inhibition, potentially though $\pi-\pi$ or π-charge interactions with Phe297 (as shown in Figure 2B). The comparison of **16** and **18** also supports this understanding. The bulkier tricyclic derivatives, **20**–**23**, displayed lower IC_{50} values than diflunisal. Among them, naphthyl derivative **22** displayed the lowest IC_{50} value of 1.32 ± 0.07 μM, though at a higher concentration (IC_{50} = 31 μM), this compound also inhibited the antiapoptotic MLC-1 protein.[33] In this case, the bulkier group may improve hydrophobic interactions that, in turn, increase inhibitory activity. In an attempt to engage a backbone amide, the 3-position of the B ring was substituted with a methanol group (**27**). The compound inhibited the enzyme with an IC_{50} value comparable to diflunisal. Further elongation of the methylene chain (**26**) weakened the inhibitory activity.

DISCUSSION

Elucidation of the Mechanism of Inhibition. Inhibition of ACMSD has been recently studied as a means of elevating the NAD^+ levels and further improving mitochondrial function as well as alleviating some diseases such as nonalcoholic fatty liver disease, steatohepatitis, acute kidney injury, and chronic kidney diseases.[3] TES-1025 inhibits ACMSD through multiple functional groups in the SAR study; however, the details regarding the mechanism of interaction remain speculative.[19] Prior to this work, the structurally determined inhibitor-binding mode involved a direct interaction between the metal and the ligand.[14,17] Typically, direct binding between a ligand and a metal center could inactivate other metalloproteins, resulting in undesirable in vivo effects. Therefore, the finding of a group of inhibitors that bind the active site of ACMSD without coordinating the catalytic zinc ion is a significant advance.

In this study, an FDA-approved drug, diflunisal, inhibits ACMSD activity by triggering two loop regions to move toward diflunisal where Arg51, Phe297, and Leu299 are located (Figure 2). Arg51 and Arg239* have been previously demonstrated to interact with the carboxylate group of the substrate during decarboxylation (Scheme 3).[15] Therefore, it is proposed that diflunisal inhibits ACMSD activity through competitive inhibition, which is supported by the inhibition assay (Figure 2D). Interestingly, Arg247*, not Arg239*, from the adjacent subunit moves to the active site and forms a salt bridge with the carboxylate group of diflunisal. This arginine residue, Arg247*, is not involved in ACMS binding and does not play a direct role in catalysis. Thus, its involvement in the inhibitor binding through structural determination deepens the molecular understanding of the ACMSD–ligand interaction mechanism. The ability of diflunisal to recruit Arg247* is unexpected. Predictably, the binding of diflunisal to the active site depends on the oligomeric status of ACMSD, like previously found for ACMS.[14−16] In the new binding mode, the molecule of diflunisal is more than 7 Å from the Zn ion (Figure 2). Since diflunisal specifically recognizes conserved residues in the active site without directly chelating the Zn ion, it may have the potential for further optimizations and drug development. Additionally, diflunisal has already been FDA-

https://dx.doi.org/10.1021/acs.jmedchem.0c01762
J. Med. Chem. 2021, 64, 797−811

Table 4. Inhibition of the Synthetic Diflunisal Derivatives

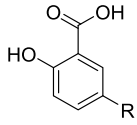

#	-R	IC_{50} (μM)	#	-R	IC_{50} (μM)
Diflunisal (**1**)	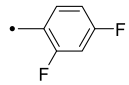	13.5 ± 0.8	TES-1025	–	0.078 ± 0.002[a]
8	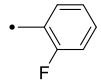	3.29 ± 0.35	**11**	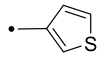	20.1 ± 1.6
10	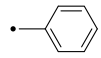 (meta-)	4.29 ± 0.27	**20**	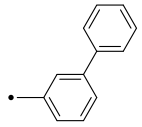	3.10 ± 0.11
13	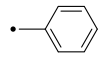 (para-)	88.0 ± 5.1	**21**	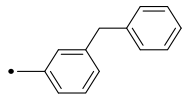	4.61 ± 0.23
16		11.1 ± 0.6	**22**	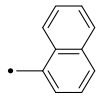	1.32 ± 0.07
17	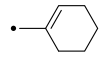	27.1 ± 2.3	**23**	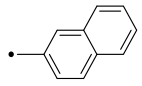	8.83 ± 0.97
18		37.3 ± 1.8	**26**	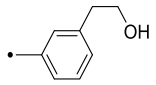	47.9 ± 2.2
19	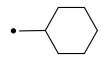	44.1 ± 2.4	**27**	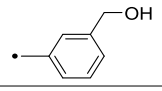	13.6 ± 1.1

[a]The IC_{50} value of TES-1025[19] was determined under the same conditions as other compounds in this study (see the Experimental Section).

approved, which reduces the likelihood for diflunisal and its derivatives to induce concerning levels of toxicity.

Insight of the Improved Inhibition of the Derivatives. Of note, diflunisal (**1**) and its derivative **11** (Figures 2 and 3) bind ACMSD in a similar binding mode in which the salicylic acid moiety interacts with Arg51 and Arg247*. In contrast, the B ring shows relative flexibility due to the weaker hydrophobic interaction. In the ACMSD structure in complex with diflunisal (Figure 2), we notice that the B ring of diflunisal orients toward a hydrophobic cavity (Figure 4) formed by Phe13, Ile43, Met45, Phe50, Val53, Leu57, Thr80, and Val82 in bacterial ACMSD (numbering Leu10, Leu39, Leu40, Phe46, Val49, Cys53, Val76, and Val78 in human ACMSD, respectively). To exploit this hydrophobic cleft, analogues bearing bulkier aromatic ring systems (**20**–**23**) displayed improved IC_{50} values. Specifically, enlarging the B ring from phenyl to naphthalene (**22**) reduced the IC_{50} value by 1 order of magnitude, from 13.5 to 1.32 μM, which could result from filling the hydrophobic cavity with the naphthalene ring. In contrast, the higher IC_{50} value of **23** (8.83 μM) could result from the different orientations of the naphthalene moiety of **23** not fitting as neatly in the hydrophobic pocket. Taken together with another derivative (**13**), the results indicate that the active-site cavity has its specific shape to embed in future inhibitor candidates.

Comparing Diflunisal with Reported Inhibitors. Diflunisal and PDC both inhibit ACMSD in a competitive manner. However, diflunisal has a 6-fold lower K_i value (2.56 ± 0.56 μM) compared with PDC (15.2 ± 0.5 μM), suggesting an improved competitive inhibitor. As shown in Figure 2, the carboxylate and hydroxyl groups interact with two Arg residues of ACMSD, of which Arg51 is involved in the catalytic reaction. Therefore, diflunisal and ACMS competitively interact with the side-chain of Arg51, which agrees well with the inhibition model indicated in Figure 2D. Pellicciari et al. developed a new cluster of inhibitors based on multiple rounds of optimization of published crystal structures of ACMSD in complex with DHAP and PDC.[19] TES-1025 (Scheme 1) exhibits an IC_{50} value of 13 nM at the 3-hydroxyanthranilic acid (3-HAA) concentration of 10 μM in a coupled assay. In this study, the substrate of ACMSD, ACMS, was prepared in a millimolar concentration by an enzymatic method.[12,34] Therefore, ACMS is directly used in the inhibition assay instead of a coupled assay. When ACMS is set at the same concentration of 10 μM as described by Pellicciari et al.,[19] the IC_{50} value for TES-1025 was measured as 0.078 ± 0.002 μM (Table 4),

https://dx.doi.org/10.1021/acs.jmedchem.0c01762
J. Med. Chem. 2021, 64, 797−811

Scheme 4. Preparation of Compounds 16−23, 26, and 27

(A) Preparation of 16–19

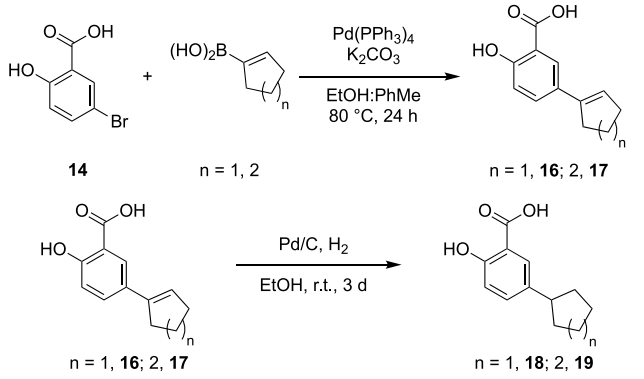

(B) Preparation of 20–23 and 26–27

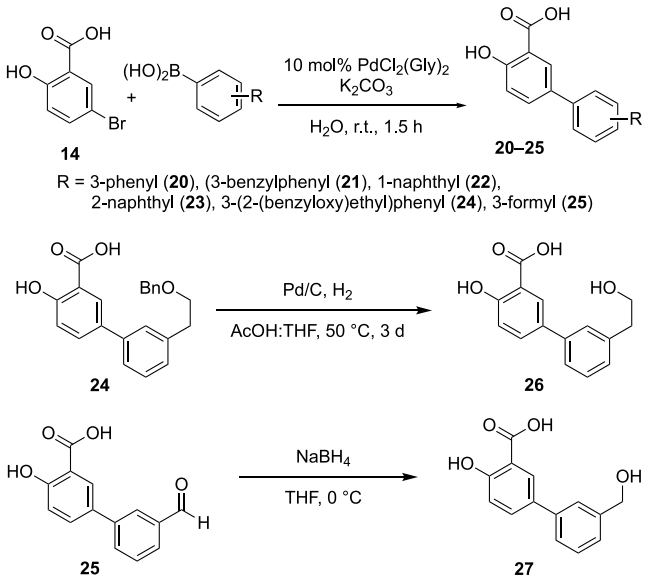

which is higher in our used method. Nonetheless, this value provides a better comparison with our diflunisal derivatives with our best hits displaying IC_{50} values of 1.32 μM (**22**) and 3.10 μM (**20**), although they are 17-fold and 40-fold weaker than TES-1025, respectively. The best hits with lower IC_{50} values, **20** and **22**, were not successfully soaked into ACMSD crystals, even after extensive attempts. However, two complex structures are still informative to reveal a new binding mode, which can be exploited in the design of future analogues.

Expanding the Understanding of Diflunisal in Regulating NAD^+ Homeostasis. Diflunisal is a derivative of salicylic acid, which is known as a nonsteroid anti-inflammatory drug. Very recently, diflunisal is reported to competitively inhibit dihydrofolate reductase.[35]

It is also a selective inhibitor of cyclooxygenase-2,[26] which is reported to be responsible for regulating inflammation and pain.[36] The elevated cyclooxygenase-2 in some cancer types suggested that it is a potential target for cancer therapy. Diflunisal derivatives with 1,2,4-triazoles on the A ring show anticancer activity toward breast cancer cells[27] and anti-inflammatory activities.[37] The iododiflunisal (on A ring) is also a potent amyloid inhibitor.[38] Here, we illustrated that diflunisal derivatives with modifications on the B ring possess an additional role in the kynurenine pathway for tryptophan degradation as an inhibitor of ACMSD. Since ACMSD inhibitors have been demonstrated to modulate NAD^+ homeostasis,[3] the results presented in this study suggest that diflunisal and its derivatives may be considered as regulators of NAD^+ biosynthesis in the tryptophan−kynurenine degradation pathway. This inhibitory effect of diflunisal and derivatives vs ACMSD should be further explored in translational repurposing studies, along with other ongoing studies evaluating diflunisal's potential for other indications.[3,19,26,35]

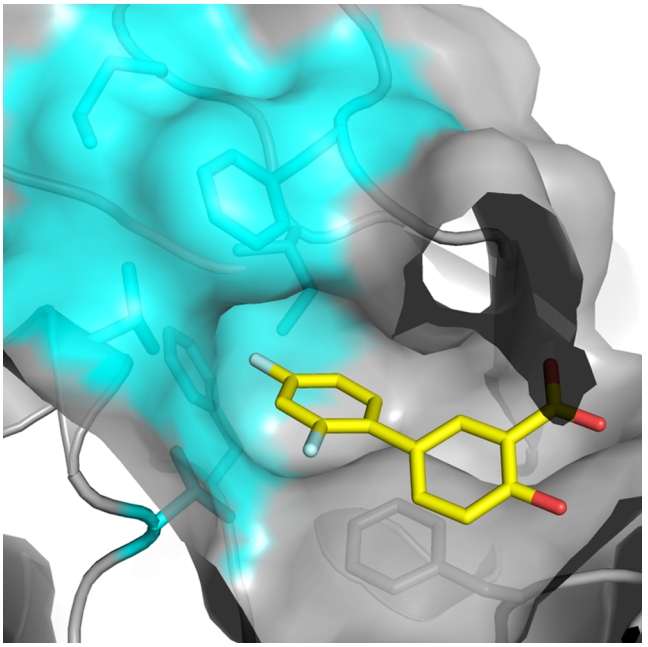

Figure 4. B ring of diflunisal points to a hydrophobic pocket (PDB entry: 7K12). The hydrophobic residues containing Phe13, Ile43, Met45, Phe50, Val53, Leu57, Thr80, and Val82 are shown in cyan. Diflunisal is shown as yellow, red, and cyan sticks for carbon, oxygen, and fluorine, respectively.

EXPERIMENTAL SECTION

Materials. Picolinic acid, quinolinic acid, acetonitrile, and trifluoroacetic acid were purchased from Sigma-Aldrich. The selected FDA-approved drugs were purchased from commercial sources [see Supporting Information (SI) for specific sources and purity data]. $PdCl_2(NH_2CH_2COOH)_2$ was prepared according to the literature.[29] 2′,4′-Difluoro-4-hydroxy-[1,1′-biphenyl]-3-carboxylic acid (diflunisal, **1**), 2′,4′-difluoro-[1,1′-biphenyl]-3-carboxylic acid (**2**), and 2′,4′-difluoro-[1,1′-biphenyl]-4-ol (**3**) were acquired from commercial sources and used without further purification. Their identity was confirmed using ^1H NMR. Unless otherwise noted, reagents were purchased from various commercial sources and used as received. All tested compounds, whether synthesized or purchased, were >95% pure as deemed by ultra performance liquid chromatography (UPLC) analysis. H_2O, used for synthetic reactions, was distilled under a N_2 atmosphere prior to use.

Protein Preparation. Human ACMSD was expressed in *Escherichia coli* with a coexpression chaperone GroEL−GroES in the M9 growth medium.[14] Isopropyl β-D-thiogalactopyranoside and L-arabinose were used to induce ACMSD and chaperone, respectively. Then, 50 μM $ZnCl_2$ was added into the medium after induction to maintain the high metal-occupancy in enzymes. The protein was purified using a nickel affinity chromatography column from the cell lysate and further purified on a Superdex 200 column with a buffer containing 25 mM *N*-(2-hydroxyethyl)piperazine-*N*′-ethanesulfonic acid (HEPES) buffer, pH 7.0, and 5% glycerol. The proteins were

https://dx.doi.org/10.1021/acs.jmedchem.0c01762
J. Med. Chem. 2021, 64, 797−811

flash-frozen in liquid nitrogen and stored at −80°C for the inhibition assay.

Methods to Screen FDA-Approved Drugs. FDA-approved drugs were downloaded from DrugBank[39] and prepared using Ligprep by Schrödinger[23] to generate ionization states around neutral pH, as well as to generate tautomers and stereoisomers (when chirality was not specified). The structure of ACMSD (PDB entry: 4IH3)[14] was downloaded and prepared using the protein preparation wizard by Schrödinger[23] to add hydrogens, identify metal-binding sites, identify ionization states, optimize hydrogen binding, and then minimize the structure into the Schrödinger's energy function. Because the asymmetric unit had six chains, that is, three dimers with six separate active sites, the minimized structure was separated into three dimers and for each dimer, a receptor docking grid was created for each of the two active sites.

The library was screened against each of the receptors using Glide[20−23] at high-throughput virtual screening (HTVS), standard precision (SP), and extra precision (XP) modes, advancing the top 20% scoring compounds, of the compounds that were able to be successfully docked at HTVS precision and the top 50% of those docket at SP precision. Poses with a score better than −10 kcal/mol at XP precision were further refined using Prime MM-GBSA,[23−25] allowing flexibility of any residue within 8 Å of the ligand. The hits from the virtual screen were filtered for pan-assay interference compounds (PAINS) (PMID 20131845) using Canvas by Schrödinger.[23,40,41]

General Synthetic Considerations. Air- and moisture-sensitive reactions were carried out in an oven-dried 1-dram vial sealed with poly(tetrafluoroethylene) (PTFE)-lined septa or glassware sealed with rubber septa under an atmosphere of dry nitrogen. PTFE syringes equipped with stainless-steel needles were used to transfer air- and moisture-sensitive liquid reagents. Reactions were stirred using Teflon-coated magnetic stir bars, and elevated temperatures were maintained using thermostat-controlled heating mantles. Organic solvents were removed using a rotary evaporator with a diaphragm vacuum pump. Thin-layer analytical chromatography was performed on silica gel UNIPLATE silica gel HLF UV254 plates, and spots were visualized by quenching of ultraviolet light (λ = 254 nm). Purification of products was accomplished by automated flash column chromatography on silica gel (VWR common silica gel 60 Å, 40−60 μm).

NMR spectra were recorded using a Bruker DRX 500 MHz (^{1}H at 500 MHz and ^{19}F at 471 MHz) or a Bruker AVIIIHD 400 MHz (^{13}C at 126 MHz) nuclear magnetic resonance spectrometer. ^{1}H NMR spectra were calibrated against the peak of the residual $CHCl_3$ (7.26 ppm), dimethyl sulfoxide (DMSO) (2.50 ppm), acetonitrile (1.94 ppm), or methanol in the solvent (4.78 and 3.31 ppm). ^{13}C NMR spectra were calibrated against the peak of the residual $CHCl_3$ (77.2 ppm) or DMSO (40.0 ppm), acetonitrile (118.7 and 1.3 ppm), or methanol in the solvent (49.0 ppm). NMR data are represented as follows: chemical shift (ppm), multiplicity (s = singlet, d = doublet, t = triplet, q = quartet, p = pentet, m = multiplet), coupling constant in hertz (Hz), and integration. High-resolution mass determinations were performed by electrospray ionization (ESI) using a Waters LCT Premier or an Agilent 6550 iFunnel Q-ToF mass spectrometer. Infrared spectra were measured using a PerkinElmer Spectrum Two Fourier transform infrared spectrometer by drying samples on a diamond attenuated total reflection (ATR) sample base plate. Uncorrected melting points were measured using a Thomas Hoover Uni-Melt capillary melting point apparatus. Retention times for liquid chromatography were recorded with a Waters H Class Plus Acquity UPLC equipped with a PDA eλ detector or Agilent 1260 Infinity II equipped with a DAD WR detector. Chromatography was performed using a 0.7 mL/min flow rate at 40 °C and Acquity UPLC ethylene-bridged hybrid (BEH) C_{18} (2.1 × 50 mm^2, 1.7 μm) column fitted with a C_{18} guard cartridge. Two mobile phase solutions were used: solution A was 0.1% formic acid in water and solution B was acetonitrile. Method A: the elution program consisted of a linear gradient starting at 98% A for 0.5 min following injection to 2% A for over 2.7 min. Method B: the elution program consisted of a linear gradient starting at 98% A for 0.5 min following injection to 2% A for over 6.5 min.

General Procedure A (Suzuki−Miyaura Coupling).[29] A 100 mL round-bottom flask equipped with a stirring bar was charged with 5-bromo-2-hydroxybenzoic acid (1.1 g, 5.0 mmol), boronic acid (6.0 mmol), $PdCl_2(NH_2CH_2COOH)_2$ (16 mg, 50 μmol), K_2CO_3 (2.1 g, 15 mmol), and H_2O (20 mL). The resulting mixture was stirred at room temperature (rt) for ∼24 h. The product precipitated upon acidification of the reaction mixture (pH ∼ 2−3, caution exothermic!), and the precipitate was collected by filtration. The solid collected was suspended in water (∼30 mL), and the pH was adjusted to 8−10 by adding 6 M NaOH dropwise (caution exothermic!). This basic mixture was heated to ∼95 °C to redissolve the solids (more water added, as needed), and the resulting solution was filtered while hot using a fritted glass funnel. The filtrate was acidified with 1 N HCl (pH ∼ 3−4, caution exothermic!) to precipitate the desired product. The product was dissolved in EtOAc and dried with Na_2SO_4. After filtration, the solvent was removed under reduced pressure, and ^{1}H NMR and UPLC analyses confirmed the identity and purity of the products. All products were dried in a high-vacuum for >6 h before testing.

*2′,4′-Difluoro-3-(hydroxymethyl)-[1,1′-biphenyl]-4-ol (**4**).* This compound was prepared according to the previous literature precedent:[42] an oven-dried two-neck round-bottom flask equipped with a stirring bar under nitrogen was charged with $LiAlH_4$ (0.30 g, 8.0 mmol). The reaction flask was cooled to 0 °C, and dry tetrahydrofuran (THF) (10 mL) was added via a syringe. Next, a solution of diflunisal (0.50 g, 2.0 mmol) in dry THF (∼5 mL) was added dropwise, and then the reaction mixture was stirred at 0 °C for 30 min. Next, the reaction mixture was refluxed for several hours until the starting material disappeared (TLC). After cooling the reaction to room temperature, the reaction was cooled to 0 °C and quenched by slow addition of 1 M HCl (5 mL). After gas evolution ceased, the product was transferred to a separation funnel and extracted with CH_2Cl_2 (3 × 25 mL). The combined organic phases were washed with $NaCl_{(sat)}$ (1 × 25 mL), dried over Na_2SO_4, filtered, and concentrated to afford the title compound as a colorless oil (0.45 g, 95%). Spectroscopic data agreed with the previous report.[42] HPLC purity 96.18%; R_t = 4.619 min (method B).

*Methyl 2′,4′-Difluoro-4-hydroxy-[1,1′-biphenyl]-3-carboxylate (**5**).* An oven-dried two-neck flask equipped with a stirring bar, a gas outlet attached to the Schlenk line, and a rubber septum under nitrogen was charged with diflunisal (0.50 g, 2.0 mmol) and CH_2Cl_2 (10 mL). The resulting suspension was cooled using an ice-water bath, and oxalyl chloride (0.19 mL, 2.2 mmol) was added. Next, dimethylformamide (DMF) (10 μL) was added dropwise (caution: rapid evolution of noxious gases). After stirring at low temperature for 10 min, the solution was stirred at room temperature until the evolution of gas ceased (mixture turned into a clear solution). Next, the reaction mixture was cooled using an ice-water bath, and NH_3 in MeOH solution (2 M, 2.0 mL, 4.0 mmol of NH_3) was added dropwise. After 10 min stirring at low temperature and 6 h at room temperature, the reaction was quenched with 1 M $HCl_{(aq)}$ (10 mL) and transferred to a separation funnel. The phases were separated, and the aqueous phase was extracted with CH_2Cl_2 (3 × 25 mL). The combined organic phases were washed with $NaCl_{(sat)}$ (1 × 25 mL), dried over anhydrous $MgSO_4$, filtered, and concentrated. Purification by flash column chromatography (20% of EtOAc in hexanes) afforded the title compound as a colorless oil (0.40 g, 75%). Spectroscopic data agreed with the previous report.[42] HPLC purity 99.99%; R_t = 6.141 min (method B).

*2′,4′-Difluoro-4-hydroxy-[1,1′-biphenyl]-3-carboxamide (**6**).* A 100 mL round-bottom flask equipped with a stirring bar was charged with **5** (0.19 g, 0.72 mmol) and MeOH (10 mL). Next, NH_4OH (7 mL, ∼30% NH_3 in H_2O) was added, and the resulting mixture was stirred at room temperature for ∼24 h. Next, the volatiles were evaporated under reduced pressure, and the aqueous residue was extracted with EtOAc (3 × 25 mL). The combined organic phases were washed with $NaCl_{(sat)}$ (1 × 25 mL), dried over anhydrous $MgSO_4$, filtered, and concentrated. Purification by flash column

https://dx.doi.org/10.1021/acs.jmedchem.0c01762
J. Med. Chem. 2021, 64, 797−811

chromatography (20−40% of EtOAc in hexanes) afforded the title compound as a colorless oil (0.15 g, 80%). Spectroscopic data agreed with the previous report.[42] HPLC purity 99.99%; R_t = 4.904 min (method B).

*4′-Fluoro-4-hydroxy-[1,1′-biphenyl]-3-carboxylic Acid (**7**).* General procedure A was followed using 5-bromo-2-hydroxybenzoic acid (1.1 g, 5.0 mmol), (4-fluorophenyl)boronic acid (0.84 g, 6.0 mmol), $PdCl_2(NH_2CH_2COOH)_2$ (16 mg, 50 μmol), K_2CO_3 (2.1 g, 15 mmol), and H_2O (20 mL). Workup and reprecipitation afforded the title compound as a colorless solid (0.79 g, 68%). Spectroscopic data agreed with the previous report.[29] HPLC purity 99.99%; R_t = 4.958 min (method B).

*2′-Fluoro-4-hydroxy-[1,1′-biphenyl]-3-carboxylic Acid (**8**).* General procedure A was followed using 5-bromo-2-hydroxybenzoic acid (1.1 g, 5.0 mmol), (2-fluorophenyl)boronic acid (0.84 g, 6.0 mmol), $PdCl_2(NH_2CH_2COOH)_2$ (16 mg, 50 μmol), K_2CO_3 (2.1 g, 15 mmol), and H_2O (20 mL). Workup and reprecipitation afforded the title compound as a colorless solid (0.78 g, 67%). Spectroscopic data agreed with the previous report.[43] HPLC purity 99.99%; R_t = 4.901 min (method B).

*3′-Fluoro-4-hydroxy-[1,1′-biphenyl]-3-carboxylic Acid (**9**).* General procedure A was followed using 5-bromo-2-hydroxybenzoic acid (1.1 g, 5.0 mmol), (3-fluorophenyl)boronic acid (0.84 g, 6.0 mmol), $PdCl_2(NH_2CH_2COOH)_2$ (16 mg, 50 μmol), K_2CO_3 (2.1 g, 15 mmol), and H_2O (20 mL). Workup and reprecipitation afforded the title compound as a colorless solid (0.59 g, 51%). ^{1}H NMR (400 MHz, MeOD) δ 8.08 (d, J = 2.4 Hz, 1H), 7.74 (dd, J = 8.7, 2.5 Hz, 1H), 7.47−7.34 (m, 2H), 7.28 (d, J = 10.6 Hz, 1H), 7.06−6.99 (m, 2H). ^{13}C{^{1}H} NMR (126 MHz, MeOD) δ 173.3, 165.7 (d, J = 244.4 Hz), 163.8, 163.1, 143.7, 143.6, 135.1, 132.1 (d, J = 2.6 Hz), 131.7 (d, J = 8.2 Hz), 129.6, 123.4 (d, J = 2.8 Hz), 118.9, 114.6 (d, J = 21.1 Hz), 114.1 (d, J = 22.0 Hz). ^{19}F NMR (470 MHz, MeOH) δ −116.46 to −116.63 (m). High-resolution mass spectrometry (HRMS) (ESI) m/z: $[M - H]^-$ calcd for $C_{13}H_8FO_3$ 231.0463; found 231.0464 (0.6 ppm). HPLC purity 99.99%; R_t = 4.928 min (method B).

*4-Hydroxy-[1,1′-biphenyl]-3-carboxylic Acid (**10**).* General procedure A was followed using 5-bromo-2-hydroxybenzoic acid (1.1 g, 5.0 mmol), phenylboronic acid (0.72 g, 6.0 mmol), $PdCl_2(NH_2CH_2COOH)_2$ (16 mg, 50 μmol), K_2CO_3 (2.1 g, 15 mmol), and H_2O (20 mL). Workup and reprecipitation afforded the title compound as a colorless solid (0.61 g, 57%). Spectroscopic data agreed with the previous report.[43] HPLC purity 99.99%; R_t = 4.861 min (method B).

*2-Hydroxy-5-(thiophen-3-yl)benzoic Acid (**11**).* Ethyl 5-bromo-2-hydroxybenzoate was prepared according to the previous literature precedent. Ethyl 5-bromo-2-hydroxybenzoate (245 mg, 1.0 mmol), 3-thiopheneboronic acid (128 mg, 1.0 mmol), $NaHCO_3$ (210 mg, 2.5 mmol), and $Pd(PPh_3)_3$ (29 mg, 25 μmol) were added to a 25 mL round-bottom flask, which was sealed with a rubber septum and placed under an Ar atmosphere. Diglyme (5.2 mL) and H_2O (2.6 mL) were injected, and the reaction mixture was heated to 105 °C and stirred for 24 h. The mixture was diluted with EtOAc (10 mL), neutralized with 1 N HCl (2.5 mL), and filtered through a pad of Celite. The mixture was washed with H_2O (10 mL) and brine (10 mL), and the organic solution was dried over Na_2SO_4, filtered, and the solvent was removed in vacuo. Reversed-phase chromatography (0.1% AcOH in H_2O/MeCN, 1:0 → 0:1) afforded the title compound as a colorless solid (42 mg, 13%). ^{1}H NMR (500 MHz, DMSO-d_6) δ 8.06 (d, J = 2.5 Hz, 1H), 7.86 (d, J = 8.7 Hz, 1H), 7.78 (s, 1H), 7.62 (s, 1H), 7.50 (d, J = 5.1 Hz, 1H), 7.00 (d, J = 8.6 Hz, 1H), 2.51−2.48 (m, 1H). ^{13}C{^{1}H} NMR (126 MHz, DMSO-d_6) δ 172.3, 160.7, 140.8, 133.8, 127.7, 127.6, 127.1, 126.4, 120.4, 118.1, 113.9. IR (film) 3681, 2982, 2866, 2844, 1667, 1033 cm^{-1}. Melting point 214.1−215.0 °C. HRMS (ESI) m/z: $[M - H]^-$ calcd for $C_{11}H_7O_3S$ 219.0116; found 219.0102 (6.4 ppm). HPLC purity 99.57%; R_t = 2.169 min (method A).

*3-Hydroxy-[1,1′-biphenyl]-4-carboxylic Acid (**13**).* 4-Bromosalicylic acid (217 mg, 1.0 mmol), phenylboronic acid (146 mg, 1.2 mmol), K_2CO_3 (415mg, 3.0 mmol), and $PdCl_2(Gly)_2$ (6.6 mg, 20 μmol) were added to a 25 mL round-bottom flask, which was sealed with a rubber septum and placed under an Ar atmosphere. H_2O (5.0 mL) was injected, and the reaction mixture was stirred at 35 °C for 1.5 h. The mixture was diluted with EtOAc (10 mL), neutralized with 1 N HCl (3.0 mL), and filtered through a pad of Celite. The mixture was washed with H_2O (20 mL) and brine (20 mL), and the organic solution was dried over Na_2SO_4, filtered, and the solvent was removed in vacuo. Reversed-phase chromatography (0.1% AcOH in H_2O/MeCN, 1:0 → 0:1) afforded the title compound as a colorless solid (150 mg, 70%). ^{1}H NMR (500 MHz, DMSO-d_6) δ 7.86 (d, J = 8.7 Hz, 1H), 7.71 (d, J = 7.2 Hz, 2H), 7.48 (t, J = 7.4 Hz, 2H), 7.42 (t, J = 7.3 Hz, 1H), 7.25−7.23 (m, 2H). ^{13}C{^{1}H} NMR (126 MHz, DMSO-d_6) δ 172.2, 161.9, 147.6, 139.2, 131.3, 129.5, 129.1, 127.4, 118.2, 115.2, 112.4. IR (film) 3052, 2847, 2557, 1777, 1650, 759, 699 cm^{-1}. Melting point 203.8−204.7 °C. HRMS (ESI) m/z: $[M - H]^-$ calcd for $C_{13}H_9O_3$ 213.0552; found 213.0566 (6.6 ppm). HPLC purity 99.99%; R_t = 2.336 min (method A).

*Lead Optimization: Synthesis of Diflunisal **16**−**29** Derivatives and Intermediates. 5-(Cyclopent-1-en-1-yl)-2-hydroxybenzoic Acid (**16**).* 5-Bromosalicylic acid (110 mg, 0.50 mmol), 1-cyclopenteneboronic acid (75 mg, 0.67 mmol), and $Pd(PPh_3)_3$ (58 mg, 50 μmol) were added to a 25 mL round-bottom flask, which was sealed with a rubber septum and placed under an Ar atmosphere. EtOH (2.1 mL), toluene (4.2 mL), and 2 M aq K_2CO_3 (4.2 mmol, 2.1 mL) were injected, and the reaction mixture was heated to 80 °C and stirred for 24 h. The mixture was diluted with EtOAc (10 mL), neutralized with 1 N HCl (4.2 mL), and filtered through a pad of Celite. The mixture was washed with H_2O (10 mL) and brine (10 mL). The organic solution was dried over Na_2SO_4, filtered, and the solvent was removed in vacuo. Reversed-phase chromatography (0.1% AcOH in H_2O/MeCN, 1:0 → 0:1) afforded the title compound as a colorless solid (20 mg, 20%). ^{1}H NMR (500 MHz, DMSO-d_6) δ 13.90 (s, 1H), 11.21 (s, 1H), 7.75 (s, 1H), 7.58 (d, J = 8.6 Hz, 1H), 6.90 (d, J = 8.6 Hz, 1H), 6.07 (s, 1H), 2.31 (s, 2H), 2.15 (s, 2H), 1.74−1.67 (m, 2H), 1.62−1.53 (m, 2H). ^{13}C{^{1}H} NMR (126 MHz, DMSO-d_6) δ 172.4, 160.4, 135.0, 133.4, 132.5, 126.2, 123.7, 117.5, 113.0, 27.1, 25.7, 23.0, 22.1. IR (film) 3681, 2959, 2865, 2844, 2619, 1651, 1445, 1199, 691, 470 cm^{-1}. Melting point 196.3−197.1 °C. HRMS (ESI) m/z: $[M - H]^-$ calcd for $C_{12}H_{11}O_3$ 203.0708; found 203.0713 (2.5 ppm). HPLC purity 99.71%; R_t = 2.428 min (method A).

*4-Hydroxy-2′,3′,4′,5′-tetrahydro-[1,1′-biphenyl]-3-carboxylic Acid (**17**).* 5-Bromosalicylic acid (108 mg, 0.50 mmol), 1-cyclohexeneboronic acid (84 mg, 0.67 mmol), and $Pd(PPh_3)_3$ (58 mg, 50 μmol) were added to a 25 mL round-bottom flask, which was sealed with a rubber septum and placed under an Ar atmosphere. EtOH (2.1 mL), toluene (4.2 mL), and 2 M aq K_2CO_3 (4.2 mmol, 2.1 mL) were injected, and the reaction mixture was heated to 80 °C and stirred for 24 h. The mixture was diluted with EtOAc (10 mL), neutralized with 1 N HCl (4.2 mL), and filtered through a pad of Celite. The mixture was washed with H_2O (10 mL) and brine (10 mL). The organic solution was dried over Na_2SO_4, filtered, and the solvent was removed in vacuo. Reversed-phase chromatography (0.1% AcOH in H_2O/MeCN, 1:0 → 0:1) afforded the title compound as a colorless solid (20 mg, 18%). ^{1}H NMR (500 MHz, DMSO-d_6) δ 13.99 (s, 1H), 11.25 (s, 1H), 7.75 (s, 0H), 7.68 (d, J = 8.6 Hz, 1H), 6.92 (d, J = 8.6 Hz, 1H), 6.16 (s, 1H), 2.62 (t, J = 7.5 Hz, 2H), 2.46 (t, J = 8.0 Hz, 2H), 1.95 (p, J = 7.5 Hz, 2H). ^{13}C{^{1}H} NMR (126 MHz, DMSO-d_6) δ 172.3, 160.7, 141.0, 133.4, 128.1, 127.0, 125.0, 117.7, 113.1, 33.3, 33.2, 23.3. IR (film) 3681, 2935, 2863, 2829, 2616, 2527, 1647, 1205, 675 cm^{-1}. Melting point 186.1−187.6 °C. HRMS (ESI) m/z: $[M - H]^-$ calcd for $C_{13}H_{13}O_3$ 217.0865; found 217.0857 (3.7 ppm). HPLC purity 99.91%; R_t = 2.524 min (method A).

*5-Cyclopentyl-2-hydroxybenzoic Acid (**18**).* 5-(Cyclopent-1-en-1-yl)-2-hydroxybenzoic acid (**16**) (580 mg, 2.8 mmol) and 5% Pd/C (30 mg, 0.28 mmol) were added to a 1-dram vial, which was sealed with a PTFE-lined septum. EtOH (3.1 mL) was injected, and the vial was placed under a H_2 atmosphere. The reaction mixture was stirred at rt for 3 days, and the mixture was diluted with MeCN (5.0 mL) and filtered through a pad of Celite. Reversed-phase chromatography (0.1% AcOH in H_2O/MeCN, 1:0 → 0:1) afforded the title compound as a colorless solid (36 mg, 6%). ^{1}H NMR (500 MHz,

https://dx.doi.org/10.1021/acs.jmedchem.0c01762
J. Med. Chem. 2021, 64, 797−811

DMSO-d_6) δ 7.62 (d, J = 2.4 Hz, 1H), 7.38 (dd, J = 8.5, 2.4 Hz, 1H), 6.86 (d, J = 8.5 Hz, 1H), 2.92 (tt, J = 9.9, 7.4 Hz, 1H), 1.98 (dddd, J = 16.8, 7.7, 4.2, 1.8 Hz, 2H), 1.80−1.69 (m, 2H), 1.68−1.56 (m, 2H), 1.46 (dddd, J = 18.3, 12.1, 6.9, 2.0 Hz, 2H). $^{13}C\{^1H\}$ NMR (126 MHz, DMSO-d_6) δ 172.4, 159.8, 136.7, 134.8, 128.4, 117.4, 113.2, 44.7, 34.6, 25.4. IR (film) 3681, 3231, 2943, 2871, 2610, 1934, 1661, 1446, 1219, 678 cm^{-1}. Melting point 146.5−147.1 °C. HRMS (ESI) m/z: $[M - H]^-$ calcd for $C_{12}H_{13}O_3$ 205.0870; found 205.0862 (3.9 ppm). HPLC purity 96.99%; R_t = 2.463 min (method A).

*5-Cyclohexyl-2-hydroxybenzoic Acid (**19**).* 4-Hydroxy-2′,3′,4′,5′-tetrahydro-[1,1′-biphenyl]-3-carboxylic acid (**17**) (40 mg, 0.18 mmol) and 5% Pd/C (2.0 mg, 18 μmol) were added to a 1-dram vial, which was sealed with a PTFE-lined septum. EtOH (0.20 mL) was injected, and the vial was placed under a H_2 atmosphere. The reaction mixture was stirred at rt for 3 days, and the mixture was diluted with MeCN (2.0 mL) and filtered through a pad of Celite. Reversed-phase chromatography (0.1% AcOH in H_2O/MeCN, 1:0 → 0:1) afforded the title compound as a colorless solid (20 mg, 50%). ^1H NMR (500 MHz, DMSO-d_6) δ 7.60 (d, J = 2.4 Hz, 1H), 7.37 (dd, J = 8.5, 2.4 Hz, 1H), 6.86 (d, J = 8.4 Hz, 1H), 2.44 (dtd, J = 11.4, 6.8, 6.1, 3.2 Hz, 1H), 1.80−1.72 (m, 4H), 1.71−1.65 (m, 1H), 1.40−1.28 (m, 4H), 1.22 (ddt, J = 12.6, 6.5, 3.3 Hz, 1H). $^{13}C\{^1H\}$ NMR (126 MHz, DMSO-d_6) δ 172.4, 159.8, 138.6, 134.7, 128.0, 117.4, 113.1, 43.1, 34.5, 26.8, 26.0. IR (film) 3681, 3255, 2982, 2922, 2854, 2624, 2581, 1918, 1663 cm^{-1}. Melting point 148.7−149.6 °C. HRMS (ESI) m/z: $[M - H]^-$ calcd for $C_{13}H_{15}O_3$ 219.1021; found 219.1010 (5 ppm). HPLC purity 97.41%; R_t = 2.600 min (method A).

*4-Hydroxy-[1,1′:3′,1″-terphenyl]-3-carboxylic Acid (**20**).* 5-Bromosalicylic acid (217 mg, 1.0 mmol), 3-biphenylboronic acid (238 mg, 1.2 mmol), K_2CO_3 (414 mg, 3.0 mmol), and $PdCl_2(Gly)_2$ (3.3 mg, 10 μmol) were added to a 10 mL round-bottom flask, which was sealed with a rubber septum and placed under an Ar atmosphere. H_2O (5.0 mL) was injected, and the reaction mixture was heated to 35 °C and stirred for 1.5 h. The mixture was diluted with EtOAc (10 mL), neutralized with 1 N HCl (1.5 mL), and filtered through a pad of Celite. The mixture was washed with H_2O (10 mL) and brine (10 mL). The organic solution was dried over Na_2SO_4, filtered, and the solvent was removed in vacuo. Reversed-phase chromatography (0.1% AcOH in H_2O/MeCN, 1:0 → 0:1) afforded the title compound as a colorless solid (44 mg, 15%), which was heated in MeOH at 70 °C to remove excess boron-containing side products, after which the residual MeOH was removed in vacuo. ^1H NMR (500 MHz, DMSO-d_6) δ 8.10 (d, J = 2.6 Hz, 1H), 7.78 (s, 1H), 7.73 (d, J = 7.5 Hz, 2H), 7.62 (dd, J = 8.4, 2.6 Hz, 1H), 7.57−7.53 (m, 2H), 7.49 (dd, J = 13.3, 7.6 Hz, 3H), 7.38 (t, J = 7.3 Hz, 1H), 6.78 (d, J = 8.4 Hz, 1H). $^{13}C\{^1H\}$ NMR (126 MHz, DMSO-d_6) δ 172.2, 163.2, 141.7, 141.3, 140.9, 130.7, 129.9, 129.4, 128.8, 128.6, 127.9, 127.3, 125.4, 125.0, 124.7, 120.6, 117.1. IR (film) 3681, 3032, 2982, 2867, 2844, 1668, 1436, 1201 cm^{-1}. Melting point 189.2−190.1 °C. HRMS (ESI) m/z: $[M - H]^-$ calcd for $C_{19}H_{13}O_3$ 289.0865; found 289.0870 (1.7 ppm). HPLC purity 99.99%; R_t = 2.676 min (method A).

*1-Benzyl-3-bromobenzene (**28**).* THF (2.0 mL) was added to a one-dram vial containing phenylmagnesium iodide (228 mg, 1.0 mmol), which was placed in a −20 °C ice bath. The mixture was allowed to cool to −20 °C, and then 3-bromobenzaldehyde (180 mg, 1.0 mmol) was injected dropwise, and the reaction mixture was stirred at rt for 2 h. The mixture was neutralized with 1 N HCl (1.0 mL) and diluted with EtOAc (2.0 mL). The mixture was washed with H_2O (2.0 mL) and brine (1.0 mL). The organic solution was dried over Na_2SO_4, filtered, and the solvent was removed in vacuo. Normal-phase chromatography (hexanes/EtOAc, 1:0 → 0:1) afforded the title compound as a colorless solid (110 mg, 42%).

The intermediate alcohol (3-bromophenyl)(phenyl)methanol (263 mg, 1.0 mmol) and dichloromethane (DCM) (0.5 mL) were added to an oven-dried 1-dram vial. $InCl_3$ (11 mg, 50 μmol), Me_2SiHCl (114 mg, 1.2 mmol), and DCM (1.0 mL) were added to a separate oven-dried 1-dram vial. The (3-bromophenyl)(phenyl)methanol solution (0.50 mL) was injected dropwise over 5 min and the reaction mixture was stirred at rt for 2 h under a N_2 atmosphere. The mixture was washed with H_2O (2.0 mL), diluted with Et_2O (2.0 mL), and filtered through a pad of Celite. The solution was dried over Na_2SO_4, filtered, and the solvent was removed in vacuo. Normal-phase chromatography (hexanes/EtOAc, 1:0 → 0:1) afforded the title compound as a colorless solid (122 mg, 49%). Spectroscopic data agreed with the previous report.[44]

*(3-Benzylphenyl)boronic Acid (**29**).* 1-Benzyl-3-bromobenzene (261 mg, 1.1 mmol) and THF (4.2 mL) were added to an oven-dried 25 mL round-bottom flask, which was sealed with a rubber septum and placed in a −76 °C ice bath under a N_2 atmosphere. The mixture was allowed to cool to −76 °C, and then 2.5 M n-BuLi (0.51 mL, 1.2 mmol) was injected dropwise. The mixture was allowed to stir at −76 °C for 1 h. Triisopropyl borate (0.64 mL, 2.8 mmol) was injected dropwise, and the reaction mixture was stirred at −76 °C for 30 min. The mixture was allowed to warm to rt and then neutralized with 1 N HCl (1.2 mL). The mixture was diluted with Et_2O (5.0 mL) and washed with H_2O (5.0 mL) and brine (5.0 mL). The solution was dried over Na_2SO_4, filtered, and the solvent was removed in vacuo. Normal-phase chromatography (hexanes/EtOAc, 1:0 → 0:1) afforded the title compound as a colorless solid (135 mg, 60%). Spectroscopic data agreed with the previous report.[45]

*3′-Benzyl-4-hydroxy-[1,1′-biphenyl]-3-carboxylic Acid (**21**).* 5-Bromosalicylic acid (115 mg, 0.53 mmol), (3-benzylphenyl)boronic acid (135 mg, 0.64 mmol), K_2CO_3 (220 mg, 1.6 mmol), and $PdCl_2(Gly)_2$ (17 mg, 53 μmol) were added to a 10 mL round-bottom flask, which was sealed with a rubber septum and placed under an Ar atmosphere. H_2O (2.7 mL) was injected, and the reaction mixture was stirred at rt for 1.5 h. The mixture was diluted with EtOAc (10 mL), neutralized with 1 N HCl (1.5 mL), and then filtered through a pad of Celite. The mixture was washed with H_2O (10 mL) and brine (10 mL). The organic solution was dried over Na_2SO_4, filtered, and the solvent was removed in vacuo. Reversed-phase chromatography (0.1% AcOH in H_2O/MeCN, 1:0 → 0:1) afforded the title compound as a colorless solid (20 mg, 12%). ^1H NMR (500 MHz, DMSO-d_6) δ 7.99 (d, J = 12.6 Hz, 1H), 7.79 (d, J = 8.6 Hz, 1H), 7.73 (d, J = 8.6 Hz, 1H), 7.52 (dd, J = 12.3, 1.8 Hz, 2H), 7.43 (t, 1H), 7.35 (t, J = 7.6 Hz, 1H), 7.31−7.26 (m, 5H), 7.19 (t, J = 6.3 Hz, 3H), 7.05 (d, J = 8.6 Hz, 0H), 6.94 (d, J = 8.7 Hz, 1H), 4.02 (s, 2H). $^{13}C\{^1H\}$ NMR (126 MHz, DMSO-d_6) δ 172.2, 164.0, 161.1, 159.1, 142.5, 141.8, 140.1, 139.7, 134.3, 133.5, 131.7, 131.5, 129.6, 129.5, 129.2, 129.2, 128.9, 128.4, 128.0, 127.7, 127.4, 127.0, 127.0, 126.4, 124.4, 124.3, 119.2, 118.3, 116.0, 41.6. IR (film) 3681, 2981, 2844, 1676, 1033 cm^{-1}. Melting point 219.1−220.2 °C. HRMS (ESI) m/z: $[M - H]^-$ calcd for $C_{20}H_{15}O_3$ 303.1021; found 303.1018 (1 ppm). HPLC purity 98.81%; R_t = 2.711 min (method A).

*2-Hydroxy-5-(naphthalen-1-yl)benzoic Acid (**22**).* 5-Bromosalicylic acid (217 mg, 1.0 mmol), 1-naphthalene boronic acid (206 mg, 1.2 mmol), K_2CO_3 (414 mg, 3.0 mmol), and $PdCl_2(Gly)_2$ (33 mg, 0.10 mmol) were added to a 25 mL round-bottom flask, which was sealed with a rubber septum and placed under an Ar atmosphere. H_2O (5.0 mL) was injected, and the reaction mixture was stirred at rt for 1.5 h. The mixture was diluted with EtOAc (10 mL), neutralized with 1 N HCl (3.0 mL), and filtered through a pad of Celite. The mixture was washed with H_2O (20 mL) and brine (20 mL). The organic solution was dried over Na_2SO_4, filtered, and the solvent was removed in vacuo. Reversed-phase chromatography (0.1% AcOH in H_2O/MeCN, 1:0 → 0:1) afforded the title compound as a purple solid (104 mg, 39%). ^1H NMR (500 MHz, DMSO-d_6) δ 8.00 (d, J = 8.0 Hz, 1H), 7.95 (d, J = 8.2 Hz, 1H), 7.85 (s, 1H), 7.79 (d, J = 8.3 Hz, 1H), 7.62 (d, J = 8.5 Hz, 1H), 7.59−7.46 (m, 3H), 7.43 (d, J = 6.9 Hz, 1H), 7.12 (d, J = 8.5 Hz, 1H). $^{13}C\{^1H\}$ NMR (126 MHz, DMSO-d_6) δ 172.2, 161.0, 138.7, 137.3, 134.0, 131.5, 131.4, 131.2, 128.9, 128.1, 127.4, 127.0, 126.4, 126.1, 125.5, 117.8, 113.7. IR (film) 3240, 2851, 2602, 2555, 1935, 1738, 1659, 1208 cm^{-1}. Melting point 224.8−225.6 °C. HRMS (ESI) m/z: $[M - H]^-$ calcd for $C_{17}H_{11}O_3$ 263.0708; found 263.0693 (5.7 ppm). HPLC purity 96.08%; R_t = 2.546 min (method A).

*2-Hydroxy-5-(naphthalen-2-yl)benzoic Acid (**23**).* 5-Bromosalicylic acid (217 mg, 1.0 mmol), 2-naphthalene boronic acid (206 mg, 1.2 mmol), K_2CO_3 (414 mg, 3.0 mmol), and $PdCl_2(Gly)_2$ (33 mg, 0.10 mmol) were added to a 25 mL round-bottom flask, which was

https://dx.doi.org/10.1021/acs.jmedchem.0c01762
J. Med. Chem. 2021, 64, 797−811

sealed with a rubber septum and placed under an Ar atmosphere. H_2O (5.0 mL) was injected, and the reaction mixture was stirred at rt for 1.5 h. The mixture was diluted with EtOAc (10 mL), neutralized with 1 N HCl (3.0 mL), and filtered through a pad of Celite. The mixture was washed with H_2O (20 mL) and brine (20 mL). The organic solution was dried over Na_2SO_4, filtered, and the solvent was removed in vacuo. Reversed-phase chromatography (0.1% AcOH in H_2O/MeCN, 1:0 → 0:1) afforded the title compound as a purple solid (164 mg, 64%). ^{1}H NMR (500 MHz, DMSO-d_6) δ 8.20 (d, J = 2.5 Hz, 1H), 8.17 (s, 1H), 7.98 (ddd, J = 10.9, 8.3, 4.1 Hz, 3H), 7.92 (d, J = 7.1 Hz, 1H), 7.81 (dd, J = 8.6, 1.9 Hz, 1H), 7.59−7.45 (m, 2H), 7.09 (d, J = 8.5 Hz, 1H). ^{13}C{^{1}H} NMR (126 MHz, DMSO-d_6) δ 172.29, 161.32, 136.92, 134.31, 133.87, 132.44, 131.30, 129.00, 128.73, 128.56, 127.93, 126.87, 126.40, 125.17, 124.89, 118.31, 114.49. IR (film) 3681, 2982, 2922, 2865, 2845, 1668 cm^{-1}. Melting point 214.4−215.9 °C. HRMS (ESI) m/z: [M − H]$^-$ calcd for $C_{17}H_{11}O_3$ 263.0708; found 263.0698 (3.8 ppm). HPLC purity 98.57%; R_t = 2.533 min (method A).

*4-Hydroxy-3′-(2-hydroxyethyl)-[1,1′-biphenyl]-3-carboxylate (**26**).* 5-Bromosalicylic acid (89 mg, 0.41 mmol), (3-(2-(benzyloxy)-ethyl)phenyl)boronic acid (128 mg, 0.50 mmol), $NaHCO_3$ (105 mg, 1.3 mmol), and $PdCl_2(Gly)_2$ (1.3 mg, 4.0 μmol) were added to a 10 mL round-bottom flask, which was sealed with a rubber septum and placed under a N_2 atmosphere. H_2O (5.0 mL) was injected, and the reaction mixture was stirred at rt for 1.5 h. The mixture was diluted with EtOAc (10 mL), neutralized with 1 N HCl (3.0 mL), and filtered through a pad of Celite. The mixture was washed with H_2O (20 mL) and brine (20 mL). The organic solution was dried over Na_2SO_4, filtered, and the solvent was removed in vacuo. Reversed-phase chromatography (0.1% AcOH in H_2O/MeCN, 1:0 → 0:1) afforded the title compound as a purple solid (41 mg, 29%).

The intermediate benzyl protected analogue 3′-(2-(benzyloxy)-ethyl)-4-hydroxy-[1,1′-biphenyl]-3-carboxylic acid (**24**) (41 mg, 0.12 mmol) and 5% Pd/C (2.5 mg, 0.02 mmol) were added to a 1-dram vial, which was sealed with a PTFE-lined septum. THF (1.2 mL) and AcOH (10 μL) were injected and the vial was placed under a H_2 atmosphere. The reaction mixture was stirred at rt for 3 days, and the mixture was diluted with MeCN (2.0 mL) and filtered through a pad of Celite and the solvent was removed in vacuo. Reversed-phase chromatography (0.1% AcOH in H_2O/MeCN, 1:0 → 0:1) afforded the title compound as a colorless solid (29 mg, 96%). ^{1}H NMR (500 MHz, acetonitrile-d_3) δ 8.09 (s, 1H), 7.76 (d, J = 7.8 Hz, 1H), 7.45 (s, 1H), 7.41 (d, J = 7.8 Hz, 1H), 7.34 (t, J = 7.6 Hz, 1H), 7.19 (d, J = 7.5 Hz, 1H), 7.02 (d, J = 8.6 Hz, 1H), 3.73 (t, J = 6.9 Hz, 2H), 2.83 (t, J = 6.9 Hz, 2H). ^{13}C{^{1}H} NMR (126 MHz, acetonitrile-d_3) δ 172.6, 161.6, 140.9, 140.2, 134.8, 132.7, 129.5, 129.0, 128.4, 127.8, 124.8, 119.3, 113.7, 63.3, 39.4. IR (film) 3707 2681, 2952, 2892, 2864, 2844, 2521, 2203, 2025, 1651 cm^{-1}. Melting point >250 °C. HRMS (ESI) m/z: [M − H]$^-$ calcd for $C_{15}H_{14}O_4$ 257.0814; found 257.0800 (3.1 ppm). HPLC purity 96.37%; R_t = 1.932 min (method A).

*4-Hydroxy-3′-(hydroxymethyl)-[1,1′-biphenyl]-3-carboxylic Acid (**27**).* 3′-Formyl-4-hydroxy-[1,1′-biphenyl]-3-carboxylic acid (**25**) (100 mg, 0.41 mmol) and $NaBH_4$ (23 mg, 0.62 mmol) were added to a 1-dram vial, which was sealed with a PTFE-lined septum. Cold THF (1.9 mL, 0 °C) was injected into the reaction mixture, which was placed in a 0 °C ice bath. The reaction mixture was cooled to 0 °C and stirred for 5 h. The mixture was quenched with 1 N HCl (1.0 mL) and allowed to warm to rt. The mixture was diluted with EtOAc (10.0 mL), and the solution was washed with H_2O (5.0 mL) and brine (5.0 mL). The organic solution was dried over Na_2SO_4, filtered, and the solvent was removed in vacuo. Reversed-phase chromatography (0.1% AcOH in H_2O/MeCN, 1:0 → 0:1) afforded the title compound as a colorless solid (41 mg, 39%), which was heated in MeOH at 70 °C to remove excess boron-containing side products, after which the residual MeOH was removed in vacuo. ^{1}H NMR (500 MHz, DMSO-d_6) δ 12.73 (s, 4H), 8.04 (s, 1H), 7.81 (d, J = 8.6 Hz, 1H), 7.56 (s, 2H), 7.48 (d, J = 7.8 Hz, 2H), 7.39 (t, J = 7.7 Hz, 1H), 7.28 (d, J = 7.5 Hz, 2H), 7.04 (d, J = 8.5 Hz, 1H), 5.24 (s, 1H), 4.56 (s, 3H). ^{13}C{^{1}H} NMR (126 MHz, DMSO-d_6) δ 172.2, 161.1, 143.8, 139.3, 134.1, 131.7, 129.2, 128.3, 125.6, 124.9, 124.6, 118.2, 114.2, 63.3. IR (film) 3681, 3364, 2973, 2866, 2844, 2596, 1672 cm^{-1}. Melting point 147.4−148.9 °C. HRMS (ESI) m/z: [M − H]$^-$ calcd for $C_{14}H_{11}O_4$ 243.0657; found 243.0645 (4.9 ppm). HPLC purity 97.33%; R_t = 1.818 min (method A).

Quantitation of Decay Products by HPLC. ACMS was synthesized by an enzymatic method described previously.[34] The candidates of ACMSD inhibitors were dissolved in either water or DMSO as stock solutions. The reaction mixture contained 100 nM human ACMSD, 40 μM ACMS, and 1 mM candidates and incubated under room temperature overnight to make sure the complete conversion to the counterpart decay products. The mixture solution was ultrafiltered to remove proteins and injected into an InertSustain C_{18} column (GL Science Inc.) on a Dionex Ultimate 3000 HPLC combined with a diode-array detector (Sunnyvale, CA). Then, the compounds of PA and QUIN were separated and detected with a mobile solution containing 2.5% acetonitrile and 0.1% trifluoroacetic acid. The PA and QUIN were calibrated with gradient concentrations.

IC_{50} and Inhibition Constant Measurement. The serial dilution of the diflunisal derivatives was premixed in the buffer containing 50 mM HEPES buffer pH 7.0 and 10 mM NaCl. The human ACMSD activity was measured by monitoring the decreasing rate of the absorbance of the substrate, ACMS, at 360 nm (ε_{360} of 47 500 M^{-1} cm^{-1}) with an Agilent 8453 diode-array spectrometer at room temperature.[11] The concentration of the substrate, ACMS, is 10 μM and is kept the same as previously reported.[12,19] The IC_{50} values were obtained as the mid-point concentration c by fitting the Boltzmann function.

The Michaelis−Menten profile of ACMSD was measured with increasing diflunisal concentrations of 1, 1.3, 5, 10, 16, and 22.5 μM. The data were globally fitted to determine the inhibition model and the inhibition constant.

Crystallization, Data Collection, Processing, and Refinement. ACMSD from *P. fluorescens* was crystallized under modified conditions,[11,16] which contains 0.2 M ammonium citrate, pH 6.4, and 15% (w/v) poly(ethylene glycol) 3350. The crystals were soaked with diflunisal derivatives for 10−30 min prior to flash-cool in liquid nitrogen. The diffraction data sets were collected at Stanford Synchrotron Radiation Laboratory (SSRL) and Structural Biology Center (SBC) and further processed and scaled using HKL-3000.[46] The complexed structures were dissolved by the molecular replacement method using ligand-free ACMSD (PDB entry 2HBV) as the template and refined using Phenix 1.10.1-2155[47] and Coot 0.8.3.[48] PyMOL was utilized in drawing structural figures.[49]

■ ASSOCIATED CONTENT

Supporting Information

The Supporting Information is available free of charge at https://pubs.acs.org/doi/10.1021/acs.jmedchem.0c01762.

Structures of compounds screened; preliminary inhibition data for compounds **11**, **16**−**23**, **26**, and **27**; docking scores for the top 50 compounds from the virtual screen; sequence alignment for human and *P. fluorescens* ACMSD; HPLC and ^{1}H NMR data for all diflunisal analogues tested; and certifications of purity for commercially acquired compounds (PDF)

Molecular formula strings (CSV)

Accession Codes

The structural coordinates for the X-ray structure of ACMSD in complex with diflunisal (**1**; PDB code 7K12) and **11** (PDB code 7K13) have been deposited to the RCSB Protein Data Base (www.rcsb.org). Authors will release the atomic coordinates upon article publication.

https://dx.doi.org/10.1021/acs.jmedchem.0c01762
J. Med. Chem. 2021, 64, 797−811

AUTHOR INFORMATION

Corresponding Authors

Aimin Liu − *Department of Chemistry, University of Texas at San Antonio, San Antonio, Texas 78249, United States;* orcid.org/0000-0002-4182-8176; Email: Feradical@utsa.edu

Ryan A. Altman − *Department of Medicinal Chemistry and Molecular Pharmacology and Department of Chemistry, Purdue University, West Lafayette, Indiana 47907, United States;* orcid.org/0000-0002-8724-1098; Email: raaltman@purdue.edu

Authors

Yu Yang − *Department of Chemistry, University of Texas at San Antonio, San Antonio, Texas 78249, United States;* orcid.org/0000-0001-5305-2435

Timothy Borel − *Department of Medicinal Chemistry, The University of Kansas, Lawrence, Kansas 66045, United States;* orcid.org/0000-0002-4632-1307

Francisco de Azambuja − *Department of Chemistry, KU Leuven, 3001 Leuven, Belgium;* orcid.org/0000-0002-5537-5411

David Johnson − *Computational Chemical Biology Core and Molecular Graphics and Modeling Laboratory, The University of Kansas, Lawrence, Kansas 66045, United States*

Jacob P. Sorrentino − *Department of Medicinal Chemistry, The University of Kansas, Lawrence, Kansas 66045, United States;* orcid.org/0000-0001-5071-5379

Chinedum Udokwu − *Department of Chemistry, University of Texas at San Antonio, San Antonio, Texas 78249, United States*

Ian Davis − *Department of Chemistry, University of Texas at San Antonio, San Antonio, Texas 78249, United States*

Complete contact information is available at: https://pubs.acs.org/10.1021/acs.jmedchem.0c01762

Author Contributions

[▽]T.B. and F.d.A. contributed equally to this work.

Notes

The authors declare no competing financial interest.

ACKNOWLEDGMENTS

This work was supported in whole or part by the National Institutes of Health (NIH) grants MH107985, GM108988 (to A.L.), and GM124661 (to R.A.A.), and the Lutcher Brown Distinguished Chair Endowment fund (to A.L.). Support for the NMR Instrumentation was provided by NIH Shared Instrumentation Grants S10OD016360 and S10RR024664, NSF Major Research Instrumentation Grants 9977422, 1625923, and NIH Center Grant P20GM103418. The contents of this publication are solely the responsibility of the authors and do not necessarily represent the official views of the National Institutes of Health.

ABBREVIATIONS

ACMS, α-amino-β-carboxymuconate-ε-semialdehyde; ACMSD, ACMS decarboxylase; 2-AMS, α-aminomuconate semialdehyde; BEH, ethylene-bridged hybrid; $CC_{1/2}$, correlation coefficient 1/2; DHAP, 1,3-dihydroxy-acetonephosphate; hACMSD, human ACMSD; 3-HAA, 3-hydroxyanthranilic acid; H-bond, hydrogen bond; HEPES, 4-(2-hydroxyethyl)-1-piperazineethanesulfonic acid; HTVS, high-throughput virtual screening; MM-GBSA, molecular mechanics-generalized Born surface area; PA, picolinic acid; PAINS, pan-assay interference compounds; PDB, protein data bank; PDC, pyridine-2,6-dicarboxylic acid; *pf*ACMSD, *P. fluorescens* ACMSD; QUIN, quinolinic acid; RMSD, root-mean-square deviation; SP, standard precision; XP, extra precision

REFERENCES

(1) Wang, Y.; Liu, K. F.; Yang, Y.; Davis, I.; Liu, A. Observing 3-hydroxyanthranilate-3,4-dioxygenase in action through a crystalline lens. *Proc. Natl. Acad. Sci. U.S.A.* **2020**, *117*, 19720−19730.

(2) Palzer, L.; Bader, J. J.; Angel, F.; Witzel, M.; Blaser, S.; McNeil, A.; Wandersee, M. K.; Leu, N. A.; Lengner, C. J.; Cho, C. E.; Welch, K. D.; Kirkland, J. B.; Meyer, R. G.; Meyer-Ficca, M. L. Alpha-amino-beta-carboxy-muconate-semialdehyde decarboxylase controls dietary niacin requirements for NAD(+) synthesis. *Cell Rep.* **2018**, *25*, 1359.e4−1370.e4.

(3) Katsyuba, E.; Mottis, A.; Zietak, M.; De Franco, F.; van der Velpen, V.; Gariani, K.; Ryu, D.; Cialabrini, L.; Matilainen, O.; Liscio, P.; Giacche, N.; Stokar-Regenscheit, N.; Legouis, D.; de Seigneux, S.; Ivanisevic, J.; Raffaelli, N.; Schoonjans, K.; Pellicciari, R.; Auwerx, J. De novo NAD^+ synthesis enhances mitochondrial function and improves health. *Nature* **2018**, *563*, 354−359.

(4) Schwarcz, R.; Whetsell, W. O., Jr.; Mangano, R. M. Quinolinic acid: an endogenous metabolite that produces axon-sparing lesions in rat brain. *Science* **1983**, *219*, 316−318.

(5) Beal, M. F.; Kowall, N. W.; Ellison, D. W.; Mazurek, M. F.; Swartz, K. J.; Martin, J. B. Replication of the neurochemical characteristics of Huntington's disease by quinolinic acid. *Nature* **1986**, *321*, 168−171.

(6) Stone, T. W.; Darlington, L. G. Endogenous kynurenines as targets for drug discovery and development. *Nat. Rev. Drug Discovery* **2002**, *1*, 609−620.

(7) Schwarcz, R. The kynurenine pathway of tryptophan degradation as a drug target. *Curr. Opin. Pharmacol.* **2004**, *4*, 12−17.

(8) Schwarcz, R.; Bruno, J. P.; Muchowski, P. J.; Wu, H. Q. Kynurenines in the mammalian brain: when physiology meets pathology. *Nat. Rev. Neurosci.* **2012**, *13*, 465−477.

(9) Muraki, T.; Taki, M.; Hasegawa, Y.; Iwaki, H.; Lau, P. C. K. Prokaryotic homologs of the eukaryotic 3-hydroxyanthranilate 3,4-dioxygenase and 2-amino-3-carboxymuconate-6-semialdehyde decarboxylase in the 2-nitrobenzoate degradation pathway of *Pseudomonas fluorescens* strain KU-7. *Appl. Environ. Microbiol.* **2003**, *69*, 1564−1572.

(10) Li, T.; Iwaki, H.; Fu, R.; Hasegawa, Y.; Zhang, H.; Liu, A. α-Amino-β-carboxymuconic-ε-semialdehyde decarboxylase (ACMSD) is a new member of the amidohydrolase superfamily. *Biochemistry* **2006**, *45*, 6628−6634.

(11) Martynowski, D.; Eyobo, Y.; Li, T.; Yang, K.; Liu, A.; Zhang, H. Crystal structure of α-amino-β-carboxymuconate-ε-semialdehyde decarboxylase: Insight into the active site and catalytic mechanism of a novel decarboxylation reaction. *Biochemistry* **2006**, *45*, 10412−10421.

(12) Li, T.; Walker, A. L.; Iwaki, H.; Hasegawa, Y.; Liu, A. Kinetic and spectroscopic characterization of ACMSD from *Pseudomonas fluorescens* reveals a pentacoordinate mononuclear metallocofactor. *J. Am. Chem. Soc.* **2005**, *127*, 12282−12290.

(13) Huo, L.; Fielding, A. J.; Chen, Y.; Li, T.; Iwaki, H.; Hosler, J. P.; Chen, L.; Hasegawa, Y.; Que, L.; Liu, A. Evidence for a dual role of an active site histidine in α-amino-β-carboxymuconate-ε-semialdehyde Decarboxylase. *Biochemistry* **2012**, *51*, 5811−5821.

(14) Huo, L.; Liu, F.; Iwaki, H.; Li, T.; Hasegawa, Y.; Liu, A. Human α-amino-β-carboxymuconate-ε-semialdehyde decarboxylase (ACMSD): A structural and mechanistic unveiling. *Proteins: Struct., Funct., Bioinf.* **2015**, *83*, 178−187.

(15) Huo, L.; Davis, I.; Chen, L.; Liu, A. The power of two: arginine 51 and arginine 239* from a neighboring subunit are essential for

catalysis in alpha-amino-beta-carboxymuconate-epsilon-semialdehyde decarboxylase. *J. Biol. Chem.* **2013**, *288*, 30862−30871.
(16) Yang, Y.; Davis, I.; Matsui, T.; Rubalcava, I.; Liu, A. Quaternary structure of α-amino-β-carboxymuconate-ε-semialdehyde decarboxylase (ACMSD) controls its activity. *J. Biol. Chem.* **2019**, *294*, 11609−11621.
(17) Garavaglia, S.; Perozzi, S.; Galeazzi, L.; Raffaelli, N.; Rizzi, M. The crystal structure of human α-amino-β-carboxymuconic-ε-semialdehyde decarboxylase in complex with 1,3-dihydroxyacetonephosphate suggests a regulatory link between NAD synthesis and glycolysis. *FEBS J.* **2009**, *276*, 6615−6623.
(18) Fukuwatari, T.; Ohsaki, S.; Fukuoka, S.-i.; Sasaki, R.; Shibata, K. Phthalate esters enhance quinolinate production by inhibiting α-amino-β-carboxymuconate-ε-semialdehyde decarboxylase (ACMSD), a key enzyme of the tryptophan pathway. *Toxicol. Sci.* **2004**, *81*, 302−308.
(19) Pellicciari, R.; Liscio, P.; Giacchè, N.; De Franco, F.; Carotti, A.; Robertson, J.; Cialabrini, L.; Katsyuba, E.; Raffaelli, N.; Auwerx, J. α-Amino-β-carboxymuconate-ε-semialdehyde decarboxylase (ACMSD) inhibitors as novel modulators of de novo nicotinamide adenine dinucleotide (NAD^+) biosynthesis. *J. Med. Chem.* **2018**, *61*, 745−759.
(20) Friesner, R. A.; Banks, J. L.; Murphy, R. B.; Halgren, T. A.; Klicic, J. J.; Mainz, D. T.; Repasky, M. P.; Knoll, E. H.; Shelley, M.; Perry, J. K.; Shaw, D. E.; Francis, P.; Shenkin, P. S. Glide: a new approach for rapid, accurate docking and scoring. 1. Method and assessment of docking accuracy. *J. Med. Chem.* **2004**, *47*, 1739−1749.
(21) Friesner, R. A.; Murphy, R. B.; Repasky, M. P.; Frye, L. L.; Greenwood, J. R.; Halgren, T. A.; Sanschagrin, P. C.; Mainz, D. T. Extra precision glide: docking and scoring incorporating a model of hydrophobic enclosure for protein-ligand complexes. *J. Med. Chem.* **2006**, *49*, 6177−6196.
(22) Halgren, T. A.; Murphy, R. B.; Friesner, R. A.; Beard, H. S.; Frye, L. L.; Pollard, W. T.; Banks, J. L. Glide: a new approach for rapid, accurate docking and scoring. 2. Enrichment factors in database screening. *J. Med. Chem.* **2004**, *47*, 1750−1759.
(23) *Schrödinger Release 2017-3: Protein Preparation Wizard; Epik; Impact; Glide; Prime*; Schrödinger LLC: New York, NY, 2018.
(24) Jacobson, M. P.; Friesner, R. A.; Xiang, Z.; Honig, B. On the role of the crystal environment in determining protein side-chain conformations. *J. Mol. Biol.* **2002**, *320*, 597−608.
(25) Jacobson, M. P.; Pincus, D. L.; Rapp, C. S.; Day, T. J. F.; Honig, B.; Shaw, D. E.; Friesner, R. A. A hierarchical approach to all-atom protein loop prediction. *Proteins: Struct., Funct., Bioinf.* **2004**, *55*, 351−367.
(26) Lu, X.; Xie, W.; Reed, D.; Bradshaw, W. S.; Simmons, D. L. Nonsteroidal antiinflammatory drugs cause apoptosis and induce cyclooxygenases in chicken embryo fibroblasts. *Proc. Natl. Acad. Sci. U.S.A.* **1995**, *92*, 7961−7965.
(27) Coşkun, G. P.; Djikic, T.; Hayal, T. B.; Türkel, N.; Yelekçi, K.; Şahin, F.; Küçükgüzel, Ş. Synthesis, molecular docking and anticancer activity of diflunisal derivatives as cyclooxygenase enzyme inhibitors. *Molecules* **2018**, *23*, No. 1969.
(28) Li, T.; Ma, J.; Hosler, J. P.; Davidson, V. L.; Liu, A. Detection of transient intermediates in the metal-dependent non-oxidative decarboxylation catalyzed by α-amino-β-carboxymuconate-ε-semialdehyde decarboxylase. *J. Am. Chem. Soc.* **2007**, *129*, 9278−9279.
(29) Liu, S.; Lv, M.; Xiao, D.; Li, X.; Zhou, X.; Guo, M. A highly efficient catalyst of a nitrogen-based ligand for the Suzuki coupling reaction at room temperature under air in neat water. *Org. Biomol. Chem.* **2014**, *12*, 4511−4516.
(30) Karplus, P. A.; Diederichs, K. Linking crystallographic model and data quality. *Science* **2012**, *336*, 1030−1033.
(31) Engh, R. A.; Huber, R. Accurate bond and angle parameters for X-ray protein structure refinement. *Acta Crystallogr., Sect. A: Found. Crystallogr.* **1991**, *47*, 392−400.
(32) Chen, V. B.; Arendall, W. B., III; Headd, J. J.; Keedy, D. A.; Immormino, R. M.; Kapral, G. J.; Murray, L. W.; Richardson, J. S.; Richardson, D. C. MolProbity: all-atom structure validation for macromolecular crystallography. *Acta Crystallogr., Sect. D: Biol. Crystallogr.* **2010**, *66*, 12−21.
(33) Petros, A. M.; Swann, S. L.; Song, D.; Swinger, K.; Park, C.; Zhang, H.; Wendt, M. D.; Kunzer, A. R.; Souers, A. J.; Sun, C. Fragment-based discovery of potent inhibitors of the anti-apoptotic MCL-1 protein. *Bioorg. Med. Chem. Lett.* **2014**, *24*, 1484−1488.
(34) Yang, Y.; Liu, F.; Liu, A. Adapting to oxygen: 3-Hydroxyanthrinilate 3, 4-dioxygenase employs loop dynamics to accommodate two substrates with disparate polarities. *J. Biol. Chem.* **2018**, *293*, 10415−10424.
(35) Duff, M. R., Jr.; Gabel, S. A.; Pedersen, L. C.; DeRose, E. F.; Krahn, J. M.; Howell, E. E.; London, R. E. The structural basis for nonsteroidal anti-inflammatory drug inhibition of human dihydrofolate Reductase. *J. Med. Chem.* **2020**, *63*, 8314−8324.
(36) Qiu, H. Y.; Wang, P. F.; Li, Z.; Ma, J. T.; Wang, X. M.; Yang, Y. H.; Zhu, H. L. Synthesis of dihydropyrazole sulphonamide derivatives that act as anti-cancer agents through COX-2 inhibition. *Pharmacol. Res.* **2016**, *104*, 86−96.
(37) Küçükgüzel, S. G.; Küçükgüzel, I.; Tatar, E.; Rollas, S.; Sahin, F.; Güllüce, M.; De Clercq, E.; Kabasakal, L. Synthesis of some novel heterocyclic compounds derived from diflunisal hydrazide as potential anti-infective and anti-inflammatory agents. *Eur. J. Med. Chem.* **2007**, *42*, 893−901.
(38) Gales, L.; Macedo-Ribeiro, S.; Arsequell, G.; Valencia, G.; Saraiva, M. J.; Damas, A. M. Human transthyretin in complex with iododiflunisal: structural features associated with a potent amyloid inhibitor. *Biochem. J.* **2005**, *388*, 615−621.
(39) Wishart, D. S.; Feunang, Y. D.; Guo, A. C.; Lo, E. J.; Marcu, A.; Grant, J. R.; Sajed, T.; Johnson, D.; Li, C.; Sayeeda, Z.; Assempour, N.; Iynkkaran, I.; Liu, Y.; Maciejewski, A.; Gale, N.; Wilson, A.; Chin, L.; Cummings, R.; Le, D.; Pon, A.; Knox, C.; Wilson, M. DrugBank 5.0: a major update to the DrugBank database for 2018. *Nucleic Acids Res.* **2018**, *46*, D1074−D1082.
(40) Sastry, M.; Lowrie, J. F.; Dixon, S. L.; Sherman, W. Large-scale systematic analysis of 2D fingerprint methods and parameters to improve virtual screening enrichments. *J. Chem. Inf. Model.* **2010**, *50*, 771−784.
(41) Duan, J.; Dixon, S. L.; Lowrie, J. F.; Sherman, W. Analysis and comparison of 2D fingerprints: Insights into database screening performance using eight fingerprint methods. *J. Mol. Graphics Modell.* **2010**, *29*, 157−170.
(42) Uusi-Oukari, M.; Vähätalo, L.; Liljeblad, A. Modifications of diflunisal and meclofenamate carboxyl groups affect their allosteric effects on GABAA receptor ligand binding. *Neurochem. Res.* **2014**, *39*, 1183−1191.
(43) Adamski-Werner, S. L.; Palaninathan, S. K.; Sacchettini, J. C.; Kelly, J. W. Diflunisal analogues stabilize the native state of transthyretin. Potent inhibition of amyloidogenesis. *J. Med. Chem.* **2004**, *47*, 355−374.
(44) Oseki, Y.; Fujitsuka, M.; Sakamoto, M.; Majima, T. Intramolecular triplet energy transfer via higher triplet excited state during stepwise two-color two-laser irradiation. *J. Phys. Chem. A* **2007**, *111*, 9781−9782.
(45) Peters, M.; Trobe, M.; Tan, H.; Kleineweischede, R.; Breinbauer, R. A modular synthesis of teraryl-based α-helix mimetics, part 1: synthesis of core fragments with two electronically differentiated leaving groups. *Chem. − Eur. J.* **2013**, *19*, 2442−2449.
(46) Otwinowski, Z.; Minor, W. [20] Processing of X-ray diffraction data collected in oscillation mode. *Methods Enzymol.* **1997**, *276*, 307−326.
(47) Adams, P. D.; Afonine, P. V.; Bunkóczi, G.; Chen, V. B.; Davis, I. W.; Echols, N.; Headd, J. J.; Hung, L.-W.; Kapral, G. J.; Grosse-Kunstleve, R. W.; et al. PHENIX: a comprehensive Python-based system for macromolecular structure solution. *Acta Crystallogr., Sect. D: Biol. Crystallogr.* **2010**, *66*, 213−221.
(48) Emsley, P.; Cowtan, K. Coot: model-building tools for molecular graphics. *Acta Crystallogr., Sect. D: Biol. Crystallogr.* **2004**, *60*, 2126−2132.

https://dx.doi.org/10.1021/acs.jmedchem.0c01762
J. Med. Chem. 2021, 64, 797−811

(49) DeLano, W. L. *The PyMOL Molecular Graphics System*, version 1.7.0.0; Schrödinger, LLC: New York, 2014.

https://dx.doi.org/10.1021/acs.jmedchem.0c01762
J. Med. Chem. 2021, 64, 797−811